

JAERI-Research
99-040



JP9950410



^{238}U OPTICAL POTENTIAL UP TO 100MeV
INCIDENT NUCLEON ENERGIES

June 1999

Efrem Sh. SUKHOVITSKII*, Satoshi CHIBA,
Osamu IWAMOTO and Tokio FUKAHORI

日本原子力研究所
Japan Atomic Energy Research Institute

本レポートは、日本原子力研究所が不定期に公刊している研究報告書です。
入手の間合わせは、日本原子力研究所研究情報部研究情報課（〒319-1195 茨城県那珂郡東海村）あて、お申し越してください。なお、このほかに財団法人原子力弘済会資料センター（〒319-1195 茨城県那珂郡東海村日本原子力研究所内）で複写による実費頒布をおこなっております。

This report is issued irregularly.

Inquiries about availability of the reports should be addressed to Research Information Division, Department of Intellectual Resources, Japan Atomic Energy Research Institute, Tokai-mura, Naka-gun, Ibaraki-ken, 319-1195, Japan.

© Japan Atomic Energy Research Institute, 1999

編集兼発行 日本原子力研究所

^{238}U Optical Potential up to 100MeV Incident Nucleon Energies

Efrem Sh. SUKHOVITSKII*, Satoshi CHIBA*,
Osamu IWAMOTO and Tokio FUKAHORI

Department of Nuclear Energy System
Tokai Research Establishment
Japan Atomic Energy Research Institute
Tokai-mura, Naka-gun, Ibaraki-ken

(Received May 12, 1999)

A coupled-channel formalism based on the axial rigid-rotor model build on a saturated coupling scheme was used for estimation of optical model potential of ^{238}U for the nucleon incident energies from 0.1 to 100MeV. Suggested best fit parameters allow description of experimental neutron and proton scattering angular distributions and neutron total cross section data almost within experimental errors. Predicted absorption cross section for neutron above 10MeV is 10% higher than adopted earlier. Use of the saturated coupling scheme allows reliable prediction of neutron transmissions for nucleon interaction with excited nuclear states (necessary for the statistical model calculation) as well as for interaction with the ground-state band.

Keywords: Coupled-channels Model, Axial Rigid-rotor Model; $^{238}\text{U}(n,n)$, (n,n') , (p,p) , (p,p') , $E=10^{-1}$ to 100MeV; Deduced Optical Model Parameters, Saturated Coupling

* Advanced Science Research Center

* Radiation Physics and Chemistry Problems Institute

^{238}U に対する100 MeV までの核子入射反応の光学模型ポテンシャル

日本原子力研究所東海研究所エネルギーシステム研究部

Bfrem Sh. SUKHOVITSKIĪ*・千葉 敏[†]・岩本 修・深堀 智生

(1999年5月12日受理)

飽和結合様式を用いる軸対称の硬回転体模型に基づくチャンネル結合理論によって、0.1 から100MeVの領域での ^{238}U の核子入射反応に対する光学模型ポテンシャルの推定を行った。中性子及び陽子の散乱断面積と中性子の全断面積をほぼ実験誤差内で記述できる光学ポテンシャルを得ることができた。このポテンシャルを用いて計算された、10MeV 以上の中性子に対する吸収断面積は従来の計算値より10%程度大きな値となった。また、飽和結合様式を用いることにより、基底状態バンドに対する断面積だけでなく、統計模型に必要な透過係数についても高精度での予測が可能となった。

東海研究所：〒319-1195 茨城県那珂郡東海村白方白根2-4

+ 先端基礎研究センター

* 放射線物理化学問題研究所

Contents

| | |
|--|---|
| 1. Introduction | 1 |
| 2. Coupled-channels Approach to Analysis of ^{238}U | 1 |
| 3. Estimation of the Optical Potential Parameters for ^{238}U | 2 |
| 4. Results and Discussion | 4 |
| 5. Concluding Remarks | 6 |
| Acknowledgments | 6 |
| References | 7 |

目 次

| | |
|---|---|
| 1. 序 論 | 1 |
| 2. チャンネル結合法による ^{238}U の断面積の解析 | 1 |
| 3. ^{238}U の光学模型パラメータの推定 | 2 |
| 4. 結果と考察 | 4 |
| 5. 結 論 | 6 |
| 謝 辞 | 6 |
| 参考文献 | 7 |

This is a blank page.

1 Introduction

The optical model is one of the fundamental theoretical tools which provides the basis of nuclear reaction data analysis and, hence, data evaluations for applied purposes. It suggests convenient approach for predictions of total, scattering and reaction cross sections. Thus it is widely used in calculations for direct reaction and quantum preequilibrium theory models, and, most importantly, in supplying particle transmission coefficients necessary in nuclear data evaluation.

To get reliable results in terms of the optical model, one needs a carefully determined set of potential parameters. Optimization of accelerator-driven minor actinide transmutation strategy requests evaluation of cross sections of a large number of actinide nuclides up to 100 MeV region, above which calculations with LAHET[1] or similar codes can be successfully applied. Below this energy, the coupled-channels (CC) calculation is required for actinides, which are highly deformed in general, to obtain the total cross sections, elastic and inelastic scattering angular distributions and transmission coefficients. Most of the coupled-channels potential suggested for actinides are based on potentials determined by Lagrange et al.[2], which was obtained to describe low energy ^{238}U experimental data, with some modifications to enhance agreement at higher energy region, e.g., total cross section from 10 up to 20MeV incident energy[3]. We made an attempt in the present work to get the optical potential for ^{238}U applicable up to 100MeV nucleon incident energies to have a tool for extending the evaluated actinide nuclear data libraries to higher incident energies.

2 Coupled-channels approach to analysis of ^{238}U

Necessary coupled-channels calculations were performed for coupling of the first $J^\pi = 0^+ \dots 8^+$ states of ^{238}U which we denote as the "saturated coupling". It was checked that inclusion of additional levels does not influence the results of calculations noticeably. One must be aware that experimental data, of course, can be described with a coupling of fewer levels. However, optical potential parameters in such a case are then moved from the "real" ones to compensate lack of coupling strength, so such optical potential parameters should be attributed to coupling scheme used and cannot guarantee reliable prediction when used with any other coupling schemes. This was the reason to use the saturated coupling in our investigations.

Automatic search procedure in code OPTMAN[4] was used for the estimation of optical potential parameters. It was assumed that the coupled states were members of $K^\pi = 0^+$ ground-state rotational band of an axially symmetric rigid-rotor.

The deformed nuclear optical potential arise from deformed instant nuclear shapes

$$R(\theta', \varphi') = R_0 \left\{ 1 + \sum_{\lambda=2,4,6} \beta_{\lambda 0} Y_{\lambda 0}(\theta', \varphi') \right\}. \quad (1)$$

The non-spherical optical potential is taken to a standard form:

$$V(r) = -V_R f_R(r) + i \left\{ 4W_D a_D \frac{d}{dr} f_D(r) - W_V f_V(r) \right\}$$

$$+ \left(\frac{\hbar}{\mu\pi c} \right)^2 V_{so} \frac{1}{r} \frac{d}{dr} f_{so}(r) \hat{\sigma} \cdot \hat{L} + V_{Coul}(r), \quad (2)$$

with the form factors given as

$$f_i(r) = [1 + \exp(r - R_i)/a_i]^{-1}, \quad i = R, V, D \text{ and } so, \quad (3)$$

and deformed radii R_i as described in Eq. (1) with $R_0 = r_i A^{1/3}$. The subscripts $i = R, V, D, Coul$ and so denote the real volume, imaginary volume, imaginary surface, Coulomb and real spin-orbit potentials, respectively, with energy dependencies given as

$$\begin{aligned} V_R &= V_R^0 + V_R^1 E_p + (-1)^{Z'+1} C_{viso}(A - 2Z)/A + ZZ'/A^{1/3} C_{coul}, \\ W_D &= W_D^0 + W_D^1 E_p + (-1)^{Z'+1} C_{wiso}(A - 2Z)/A, \\ W_V &= W_V^0 + W_V^1 E_p \end{aligned} \quad (4)$$

where E_p is energy of the projectile and W_i^1 changing at $E_p = E_{change}$, while Z' and Z are charges of incident particle and nucleus, respectively, and A denotes mass number of the target nucleus.

The Coulomb potential $V_{Coul}(r)$ was calculated using a multipole expansion of the Coulomb potential V_{Coul} for charged ellipsoid with a uniform charge density within the Coulomb radius R_C and zero outside, as suggested by Satchler et al.[5]. For axial nuclei, up to the second order of $\sum \beta_{\lambda 0} Y_{\lambda 0}$ it reads

$$\begin{aligned} V_{Coul} &= \frac{ZZ'e^2}{2R_c} \left[3 - \frac{r^2}{R_c^2} \right] \theta(R_C - r) + \frac{ZZ'e^2}{r} \theta(r - R_C) \\ &+ \sum_{\lambda} \frac{3ZZ'e^2}{2\lambda + 1} \left[r^{\lambda} R_C^{-(\lambda+1)} \theta(R_C - r) + R_C^{\lambda} r^{-(\lambda+1)} \theta(r - R_C) \right] (\beta_{\lambda 0} Y_{\lambda 0}) \\ &+ \sum_{\lambda} \frac{3ZZ'e^2}{2\lambda + 1} \left[(1 - \lambda) r^{\lambda} R_C^{-(\lambda+1)} \theta(R_C - r) + (\lambda + 2) R_C^{\lambda} r^{-(\lambda+1)} \theta(r - R_C) \right] \\ &\cdot \sum_{\lambda' \lambda''} \frac{\hat{\lambda}' \hat{\lambda}''}{(4\pi)^{1/2} \hat{\lambda}} (\lambda' \lambda'' 00 | \lambda 0) (\beta_{\lambda'} \otimes \beta_{\lambda''})_{\lambda 0} Y_{\lambda 0} \end{aligned} \quad (5)$$

where $\hat{\lambda} = (2\lambda + 1)^{1/2}$, while the symbol \otimes means the vector addition, i.e.,

$$(\beta_{\lambda'} \otimes \beta_{\lambda''})_{\lambda 0} = (\lambda' \lambda'' 00 | \lambda 0) \beta_{\lambda' 0} \beta_{\lambda'' 0}, \quad (6)$$

and $\theta(r) = 1$ if $r > 0$ and $\theta(r) = 0$ if $r < 0$.

Our Coulomb potential includes some modifications to the formula (5). Spherical term of it was calculated taking account of diffuseness of charge distribution. Moreover, we truncated the square terms $(\beta_{\lambda'} \otimes \beta_{\lambda''})_{\lambda 0} Y_{\lambda 0}$ which lead to zero Coulomb multipoles. This is necessary for the nuclear volume conservation[6].

As we intended to analyze neutron and proton scattering data simultaneously, our potential contains a term $ZZ'/A^{1/3} C_{coul}$ describing the Coulomb correction to the real optical potential and isospin terms $(-1)^{Z'+1} C_{viso}(A - 2Z)/A$ added to real and $(-1)^{Z'+1} C_{wiso}(A - 2Z)/A$ to imaginary surface potentials.

3 Estimation of the optical potential parameters for ^{238}U

The following experimental scattering data were involved in the current analysis: scattering data by Haouat et al. for excitation of resolved 0^+ , 2^+ and 4^+ levels for incident neutron energy 3.4MeV[8];

scattering data by Smith and Chiba for excitation of a sum of 0^+ , 2^+ , 4^+ , 6^+ and 8^+ levels for twelve incident neutron energies from 4.5 to 10.0 MeV[9]; scattering data by Kinney et al. for excitation of a sum of 0^+ , 2^+ , 4^+ , 6^+ and 8^+ levels for incident neutron energies 6.44, 7.54 and 8.56 MeV[10]; scattering data by Baba et al. for excitation of a sum of 0^+ , 2^+ , 4^+ , 6^+ and 8^+ levels for incident neutron energy 6.1 MeV[11]; scattering data by Kammerdiener for excitation of a sum of 0^+ , 2^+ , 4^+ , 6^+ and 8^+ levels for incident neutron energy 14.1 MeV[12]; scattering data by Hansen et al. for excitation of a sum of 0^+ , 2^+ , 4^+ , 6^+ and 8^+ levels for incident neutron energy 14.1 MeV[13]; scattering data by Shen et al. for excitation of a sum of 0^+ , 2^+ , 4^+ , 6^+ and 8^+ levels for incident neutron energy 14.2 MeV[14]; scattering data by Hansen et al. for excitation of resolved 0^+ , 2^+ , 4^+ and 6^+ levels for incident proton energies at 20 and 26 MeV[15]; scattering data by King et al. for excitation of resolved 2^+ , 4^+ and 6^+ levels for incident proton energy of 35 MeV[16]; scattering data by Takeuchi et al. for excitation of resolved 0^+ , 2^+ , 4^+ and 6^+ levels for incident proton energy 65 MeV[17]. Available scattering data with neutron incident energies below 3.4 MeV were not used in this investigation, as for such low energies data contain compound contribution, that is significant and cannot be neglected while optical parameter search. For chosen scattering experimental data we could assume that the interaction of nucleons with ^{238}U proceeds only via the direct mechanism and could organize optical parameter search comparing experimental data with optical model coupled-channels calculations.

Evaluated neutron strength functions $S_0 = (1.10 \pm 0.08) \times 10^{-4} (\text{eV})^{-1/2}$ [18] and $S_1 = (2.0 \pm 0.5) \times 10^{-4} (\text{eV})^{-1/2}$ [19] and potential scattering radius $R' = (9.44 \pm 0.35) \text{ fm}$ [19] were also used in parameter search. Evaluated total neutron cross section with associated errors for energies from 0.250 up to 90 MeV[19, 20] was also used in optical parameter search instead of experimental total cross section as it shows scatter from smooth evaluated values. In addition to energy points in which experimental neutron scattering data exist, total cross sections at 0.250, 1.3, 20, 29, 40, 50, 65 and 90 MeV were included in the potential search. As a result, the total cross section data considered cover all the critical energy points which are necessary to reveal the structure due to the Ramsauer effect. A detailed information about the data used in the CC analysis is found in Table 1.

The optical potential parameters were searched for by minimizing the quantity χ^2 defined by

$$\chi^2 = \frac{1}{N + M + 3} \left[\sum_{i=0,1} \left(\frac{S_{i,calc} - S_{i,eval}}{\Delta S_{i,eval}} \right)^2 + \left(\frac{R'_{calc} - R'_{eval}}{\Delta R'_{eval}} \right)^2 + \sum_{i=1}^N \frac{1}{K_i} \sum_{j=1}^{K_i} \left(\frac{d\sigma_{ij}/d\Omega_{calc} - d\sigma_{ij}/d\Omega_{exp}}{\Delta d\sigma_{ij}/d\Omega_{exp}} \right)^2 + \sum_{i=1}^M \left(\frac{\sigma_{tot,cal_i} - \sigma_{tot,eval_i}}{\Delta \sigma_{tot,eval_i}} \right)^2 \right] \quad (7)$$

where N denotes number of experimental scattering data sets, K_i number of angular points in each scattering data set, M number of energies for which experimental neutron total cross section is involved. The optical potential parameters allowing the best fit to the experimental data are presented in Table 2.

4 Results and discussion

It is evident that the total neutron cross section data for ^{238}U in the energy region from 0.1 up to 100 MeV (Fig. 1) and experimental neutron and proton scattering data (Figs. 2 to 34) are described fairly well by the suggested optical model parameters. The χ^2 are 1.66 for neutron and 3.15 for proton experimental data. Overall χ^2 is 2.14. The χ^2 calculated for the same experimental data base and optical parameters[3] is 11.2. One can see that our optical potential parameters describe experimental data much better than potentials suggested by Lagrange et al.[2] and Young et al. [3]. The reason is as follows. There is only one energy point at 3.4 MeV in the neutron data with resolved scattering with excitation of the first three levels 0^+ , 2^+ and 4^+ . As we used both neutron and proton scattering data in our potential search, we involved in our search a number of proton experimental points with resolved excitation of 0^+ , 2^+ , 4^+ and 6^+ levels. Coupling strength of these states and thus scattering cross sections are approximately proportional to square of deformations multiplied by derivatives of potential form-factors. Account of experimental scattering data for resolved levels leads to much more reliable determination of optical potential parameter geometry in our case, especially deformations $\beta_{\lambda 0}$ and diffuseness a_i . Furthermore, the proton scattering data covers energy region from 20 up to 65 MeV, not covered by neutron experiments except for the total cross section, allowing to fix energy dependences of the potential parameters reliably.

It is interesting to compare the absorption cross sections predicted by different potentials. Here, the absorption cross section is defined as the difference between total cross section and sum of direct scattering cross sections. One can see that our potential parameters predict much higher one (Fig. 35) than predicted by the Youngs's potential above several MeV. To check the reliability of this prediction, we repeated our search procedure several times starting from different initial optical parameter sets and we got the same best fit ^{238}U optical parameters each time. So we concluded that available experimental data indicates high absorption cross section.

The experimental angular distributions of all the scattered proton data, and scattered neutrons with incident energies 7.54, 8.56[10], 7.5, 8.03, 8.4, 9.06, 9.5, 10.0[9] and in the vicinity of 14 MeV[12, 15, 14], measured for the energy loss less than 1 MeV, are in fact differential cross sections of direct scattering because the contribution of compound-nucleus mechanism for scattering with the above-mentioned energy loss does not exceed 0.001 barn above projectile energy of several MeV. Our optical potential allows to describe consistently both experimental total and scattering cross sections, while potentials [2, 3] underestimate total cross section and display tendency to overestimate back-angle cross section for higher incident energies. This explains the difference in absorption cross section predictions and gives us confidence that our high absorption values are grounded on experimental data. Moreover, according to Anikin et al.[21] the most probable values of the total cross section for interaction of neutrons with ^{238}U nuclei should be closer to the upper edge of the spread band of experimental values, this also supports higher absorption.

It should be noted that the difference in predicted absorption cross section could substantially affect the results of statistical (n,Xn) and (n,Xnf) cross sections predictions. This is particularly important

for strongly fissile nuclei for which first chance non-emissive fission cross section σ_{nf} amounts to a half of the absorption cross section for incident energies 10-20 MeV. Since the relative difference of the $\sigma_{abs} - \sigma_{nf}$ cross section values is larger than that of the σ_{abs} alone by about a factor of 2 or more, the relative difference in (n,Xn) process ($X \geq 2$) and (n,Xnf) for $X \geq 1$ will be twice or more larger than the relative difference in predicted absorption cross sections σ_{abs} . Absorption cross section and the fraction of preequilibrium emission determine cross section of preequilibrium emission. The latter in fact was fixed for actinides from comparison with the neutron emission spectra, the high-energy tail of the (n,2n) reaction cross section, and other experimental quantities in the vicinity of 14MeV for ^{238}U [22]. Hence, the nuclear model parameters can be changed significantly as a result of fitting them to experimental data using changed absorption cross section. This would in turn change the cross sections predicted by these models for minor actinides, for which no experimental data are available.

Nevertheless we must keep in mind that standard axial rigid-rotor CC optical model approach has inherent drawback that can lead to ~ 0.2 barn overestimation of reaction cross section in the vicinity of 3.5 MeV incident energy. The thing is that axial rigid-rotor CC approach takes into account coupling of ground state rotational band only. While last Geel[23] experiments showed that for neutron incident energy 3.51 MeV, cross section of level excitation with energy losses $E_X = 0.63-0.89$ and $0.89-1.32$ MeV are 0.056 ± 0.012 and 0.18 ± 0.05 barn, respectively. One can easily check that for such incident energy ^{238}U levels with the quoted excitations are excited through direct mechanism, impact of compound process is less than $\sim 5\%$. That means that levels from other than ground state bands are excited via direct mechanism. For the first $E_X = 0.63 - 0.89$ MeV group these are levels of $K \simeq 0^-$ band and for $E_X = 0.89 - 1.32$ MeV levels of $K \simeq 2^+$ and higher $K \simeq 0^+$ bands. So measured direct excitation cross section of levels from other than ground state band is more than half of the measured $J^\pi = 2^+$ ground state level excitation [8] and thus cannot be ignored.

We are developing soft-rotator CC approach[7, 24, 25, 26], which allows the account of coupling of all the excited levels including negative $K \simeq 0^-$ band. In case of ^{238}U we can describe collective excitations and couple them for coupled-channels calculations up to excitation energies ~ 2 MeV. Preliminary calculations with coupling including main levels of three rotational bands other than ground state show that soft-rotator model predictions are in good agreement with Geel experimental data [23]. Calculated cross section of level excitation with energy loss $E_X = 0.89-1.32$ MeV is ~ 0.20 barn and is mainly the sum of $K \simeq 2^+$ band $2^+(1.0603 \text{ MeV}) = 0.13$ barn, $3^+(1.1056\text{MeV}) = 0.01$ barn, $4^+(1.1677\text{MeV}) = 0.03$ barn level excitations and excitation of six levels from two higher $K \simeq 0^+$ bands, each less than 0.01barn. Calculated cross section of negative parity band level excitation with energy loss $E_X = 0.63 - 0.89$ MeV is ~ 0.04 barn.

Axial rigid-rotor and non-axial soft-rotator based CC approach optical models with fitted optical parameters predict the same experimental total cross section and direct scattering cross section with excitation of ground state band levels. In the vicinity of 3.5 MeV incident energy non-axial soft-rotator optical model predicts additional ~ 0.24 barn direct scattering cross section on levels other than ground state band. Hence, the absorption cross section predicted by the soft-rotator CC approach in the vicinity

of 3.5 MeV will be lower than the prediction of the axial rotor CC by this amount. Such difference in absorption cross section predicted by both models decreases with the growth of neutron incident energy, as cross section of level excitation from other bands decreases with the energy and is ~ 0.05 barn for neutron incident energy ~ 14 MeV.

To our regret we are not ready to demonstrate final results for soft-rotator model in this paper. Such calculations are very time consuming, as we need to include a lot of additional levels in coupling scheme and we still have no unique ^{238}U optical potential for incident neutrons up to 100 MeV.

5 Concluding remarks

We have used a saturated coupling scheme for the analysis of nucleon + ^{238}U interaction so that the optical parameters are not influenced by lack of coupling for axial rigid-rotor case. This means that potential suggested can be used for analyses of nucleon interaction with excited (states of the ground state rotational band) ^{238}U nuclei, as such calculations involve rebuild coupling scheme, predicting correct nucleon transmissions for outgoing nucleons leaving nuclei excited. Such transmissions are necessary for account of competing nucleon emitting channels in statistical model calculations.

Acknowledgments

The authors are grateful to Dr. Akira Hasegawa of JAERI Nuclear Data Center for helpful comments on this work.

References

- [1] R.E. Prael, Proc. Int. Symp. Nuclear Data Evaluation Methodology, Brookhaven, USA, October 12-16, 1992, p.525, World Scientific (1993).
- [2] G. Haouat, J. Lachkar, Ch. Lagrange et al., Nucl. Sci. Eng. **81**, 491 (1982).
- [3] P.G. Young, Handbook for Calculations of Nuclear Reaction Data, IAEA-TECDOC-1034, p.131, Vienna (1998).
- [4] E.Sh. Sukhovitskiĭ, Yu.V. Porodzinskiĭ, O. Iwamoto, S. Chiba and K. Shibata, Report JAERI-Data/Code 98-019, JAERI (1998).
- [5] R.H. Bassel, R.M. Drisko and G.R. Satchler, Oak Ridge National Laboratory Report ORNL-3240, (1962)(unpublished).
- [6] J.M. Eisenberg and W. Greiner, "Nuclear Models", North-Holland, Amsterdam (1970).
- [7] E.Sh. Sukhovitsiĭ, S. Chiba, O. Iwamoto and Yu.V. Porodzinskiĭ, Nucl. Phys. **A640**, 147 (1998).
- [8] G. Haouat, J. Lachkar, Ch. Lagrange, Y. Patin, J. Sigauo and R.E. Shamu, Report NEANDC(E) 196 "L" (1978).
- [9] A.B. Smith and S. Chiba, Ann. Nucl. Energy **23**, 459 (1996).
- [10] W.E. Kinney and F.G. Perey, Report ORNL-4804 (1973).
- [11] M. Baba, H. Wakabayashi, N. Ito, K. Maeda and N. Hirakawa, Report JAERI-M 89-143 (1989).
- [12] J.L. Kammerdiener, Report UCRL-51232 (1972).
- [13] L.F. Hansen, B.A. Pohl, C. Wong, R.C. Haight and Ch. Lagrange, Phys. Rev. **C34**, 2075 (1986).
- [14] Shen Guanran, Huang Tangzi, Wen Shenlin, Yu Chunying, Li Anli, Tang Hongqing, Shen Qingbiao, Zhao Zhixinag and Gu Fuhua, Chinese J. of Nucl. Phys. **6**, 193 (1984).
- [15] L.F. Hansen, I.D. Proctor, D.W. Heikkinen and V.A. Madsen, Phys.Rev. **C25**, 189 (1982).
- [16] C.H. King, J.E. Finck, G.M. Grawley, J.A. Nolen, Jr. and R.M. Ronningen, Phys. Rev. **C20**, 2084(1979).
- [17] Y. Takeuchi, H. Sakaguchi, M. Nakamura, T. Ichihara, M. Yosoi, M. Ieiri and S. Kobayashi, Phys. Rev. **C34**, 493 (1986).
- [18] Yu.V. Porodzinskiĭ and E.Sh. Sukhovitskiĭ, JAERI-Conf 97-001, p.34 (1997).
- [19] Cross Section Evaluation Working Group, *ENDF/B-VI Summary Documentation*, Report BNL-NCS-17541 (ENDF201) (1991), edited by P.F. Rose, National Nuclear Data Center, Brookhaven National Laboratory, Upton, NY, USA.

- [20] V.McLane, C.L. Dunford and P.F. Rose, Neutron Cross Sections (Academic, New York, 1988), Vol.2.
- [21] G.V. Anikin, A.G. Dovbenko and I.I. Kotukhov, Vopr. At. Nauki Tekh., Ser:Yad. Konstanty, Moskow: TsNIIatominform, No. 4, 3 (1985).
- [22] A.V. Ignatyuk, V.M. Maslov and A.B. Paschenko, Yad. Fiz., 47, 355 (1988).
- [23] C. Goddio, A.J.M. Plompen and E. Wattecamps, Proc. Int. Conf. on Nucl. Data for Sci. and Tech., Trieste, May, 1997, v.1, p.532; more detailed information in: Report to WPMA/WPEC Meeting, Antwerpen, 1998.
- [24] Y.V. Porodzinskiĭ and E.Sh. Sukhovitskiĭ, Phys. of Atomic Nuclei, 59, 228 (1996)
- [25] S. Chiba., O. Iwamoto, Y. Yamanouti, M. Sugimoto, M. Mizumoto, K. Hasegawa, E.S. Sukhovitskiĭ, Y.V. Porodzinskiĭ, and Y. Watanabe, Nucl. Phys. **A624**, 305(1997).
- [26] E.Sh. Sukhovitskiĭ, S. Chiba, and O. Iwamoto, Nucl. Phys. **A 646**, 19(1999).

Table 1: Experimental scattering data involved in CC optical analysis

| Reference | Projectile | Energy (MeV) | Spin, parity, energy of the excited level | | | | |
|---------------------|------------|-----------------|---|------------------------|------------------------|------------------------|---|
| | | | 0 ⁺ (0.0) | 2 ⁺ (0.044) | 4 ⁺ (0.148) | 6 ⁺ (0.307) | \sum 0 ⁺ ...8 ⁺ |
| Haoaut et al.[8] | n | 3.4 | o | o | o | | |
| Smith and Chiba[9] | n | 4.5 | | | | | o |
| | | 5.0 | | | | | • |
| | | 5.5 | | | | | • |
| | | 5.9 | | | | | o |
| | | 6.5 | | | | | • |
| | | 7.14 | | | | | • |
| | | 7.5 | | | | | o |
| | | 8.03 | | | | | • |
| | | 8.4 | | | | | • |
| | | 9.06 | | | | | • |
| | | 9.5 | | | | | • |
| Kinney et al.[10] | n | 6.44 | | | | | • |
| | | 7.54 | | | | | • |
| | | 8.56 | | | | | o |
| Baba et al.[11] | n | 6.1 | | | | | o |
| Kammerdiener[12] | n | 14.1 | | | | | o |
| Hansen et al.[13] | n | 14.1 | | | | | o |
| Shen et al.[14] | n | 14.2 | | | | | o |
| Hansen et al.[15] | p | 20.0 | o | o | o | | |
| | | 26.0 | o | o | o | o | |
| King et al.[16] | p | 35.0 | | o | o | o | |
| Takeuchi et al.[17] | p | 65.0 | o | o | o | o | |

o- data used for potential parameter adjustment

•- data used for comparison only

Table 2: The optical potential parameters allowing the best fit of experimental data

| | | |
|--|--|------------------------|
| $V_R = 46.65 - 0.307E + 0.001E^2$ | | |
| $W_D = \begin{cases} 4.49 + 0.491E & E \leq 11.2 \\ 9.99 - 0.071(E - 11.2) & E > 11.2 \end{cases}$ | | |
| $W_V = \begin{cases} 0.0 & E \leq 11.2 \\ 0.100(E - 11.2) & E > 11.2 \end{cases}$ | | |
| $V_{so} = 6.02$ | | |
| $r_R = 1.2616$ | $a_R = 0.643$ | |
| $r_D = 1.2331$ | $a_D = \begin{cases} 0.567 + 0.0022E & E \leq 11.2 \\ 0.5916 & E > 11.2 \end{cases}$ | |
| $r_V = 1.245$ | $a_V = 0.324$ | |
| $r_C = \begin{cases} 1.23 & E \leq 25 \\ 1.23 - 0.0181(E - 25) & 25 > E > 35 \\ 1.049 & E \geq 35 \end{cases}$ | $a_C = 0.291$ | |
| $C_{Coul} = 0.366$ | $C_{viso} = 5.0$ | $C_{wiso} = 9.0$ |
| $r_{so} = 1.12$ | $a_{so} = 0.59 - 0.002E$ | |
| $\beta_{20} = 0.219$ | $\beta_{40} = 0.053$ | $\beta_{60} = -0.0065$ |

Strength and incident energy E in MeV; radii and diffusenesses in fm.

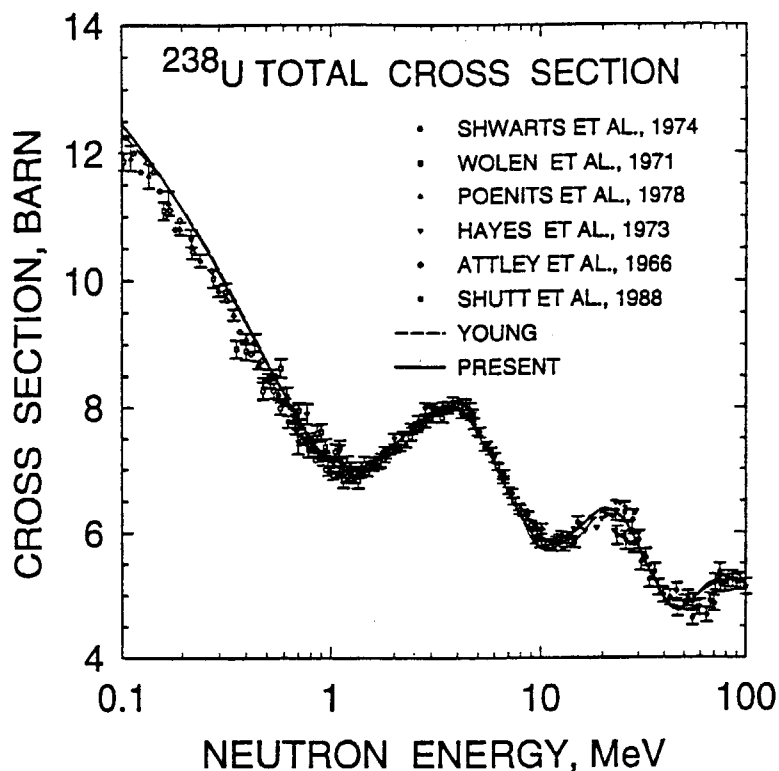


Fig. 1. Neutron total cross section of ^{238}U from 0.1 to 100 MeV. The solid line denotes the result calculated by the optical potential obtained in this work, while the broken curve is obtained with Young's potential. Experimental data are shown by various symbols.

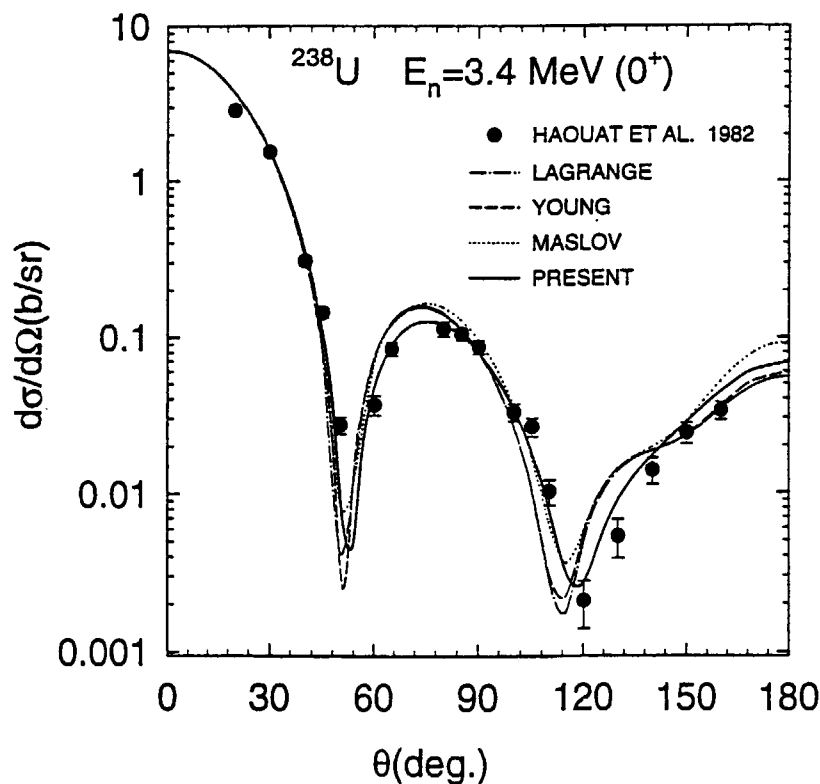


Fig. 2. Neutron elastic scattering cross section of ^{238}U at 3.4 MeV. The full circles denote experimental data obtained by Haouat et al. Various lines are the results of CC calculations : present OMP (solid line), OMP of Lagrange (dash-dotted line), OMP of Young (broken line), and OMP of Maslov (dotted line).

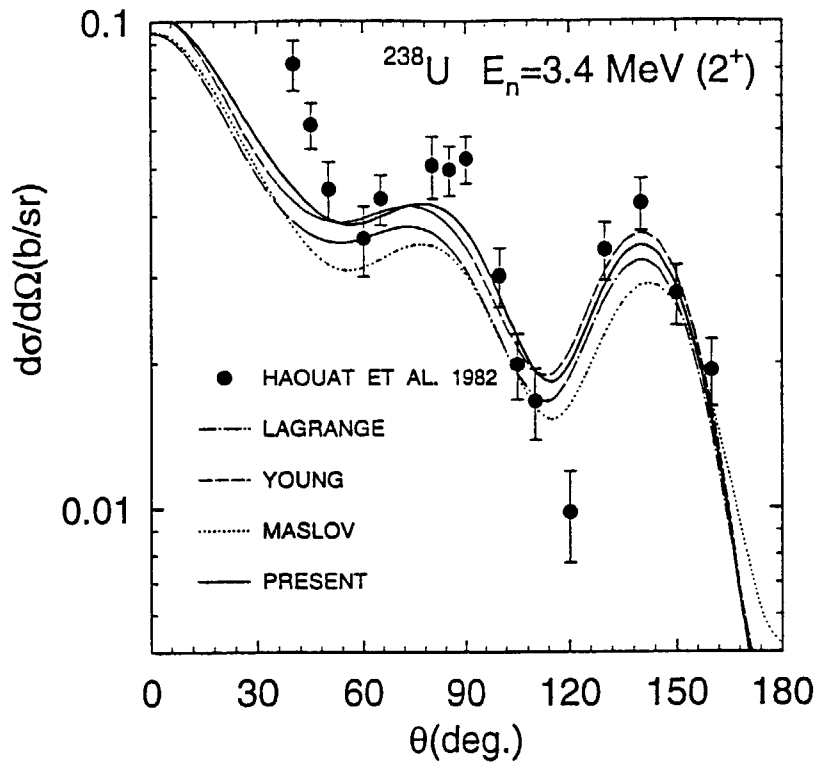


Fig. 3. Neutron inelastic scattering cross section to the 1st excited state (2^+) of ^{238}U at 3.4 MeV. Meaning of the symbol and lines are the same as in Fig. 2.

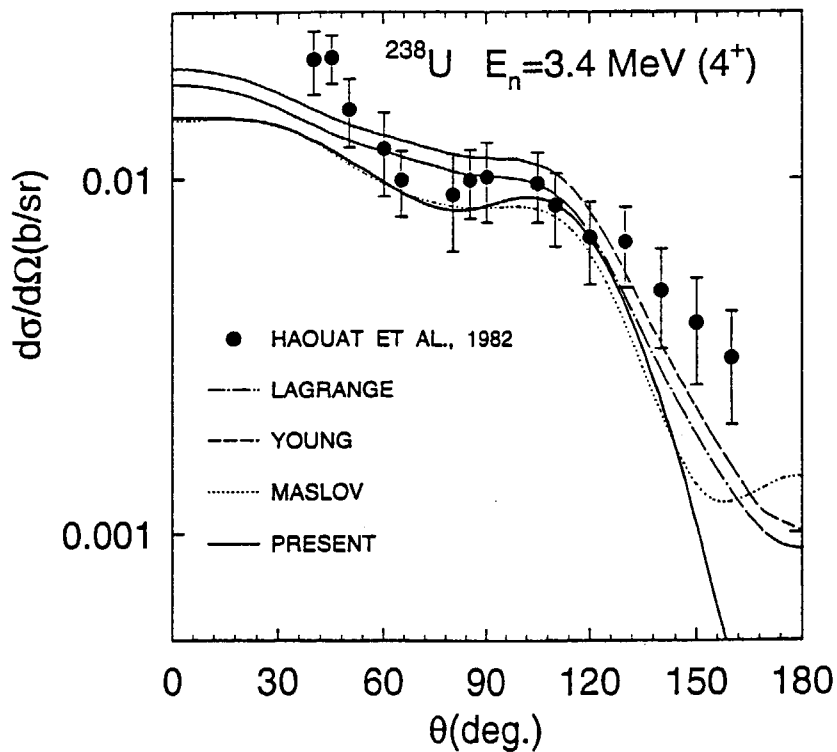


Fig. 4. Neutron inelastic scattering cross section to the 2nd excited state (4^+) of ^{238}U at 3.4 MeV. Meanings of the symbol and lines are the same as in Fig. 2.

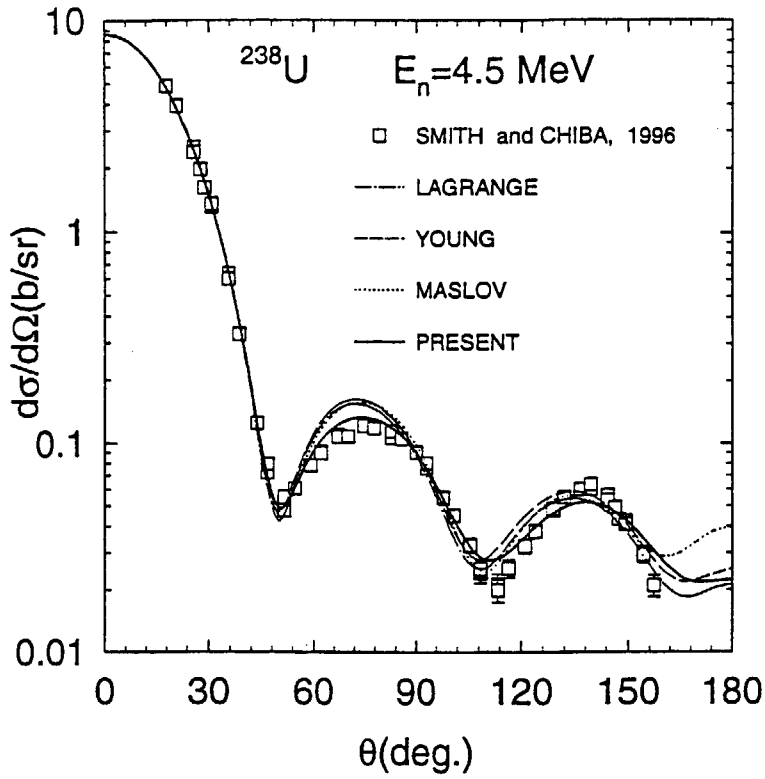


Fig. 5. Neutron scattering cross section for excitation of a sum of 0^+ , 2^+ , 4^+ , 6^+ and 8^+ levels of ^{238}U at 4.5 MeV. The open squares denote experimental data obtained by Smith and Chiba. Meanings of the lines are the same as in Fig. 2.

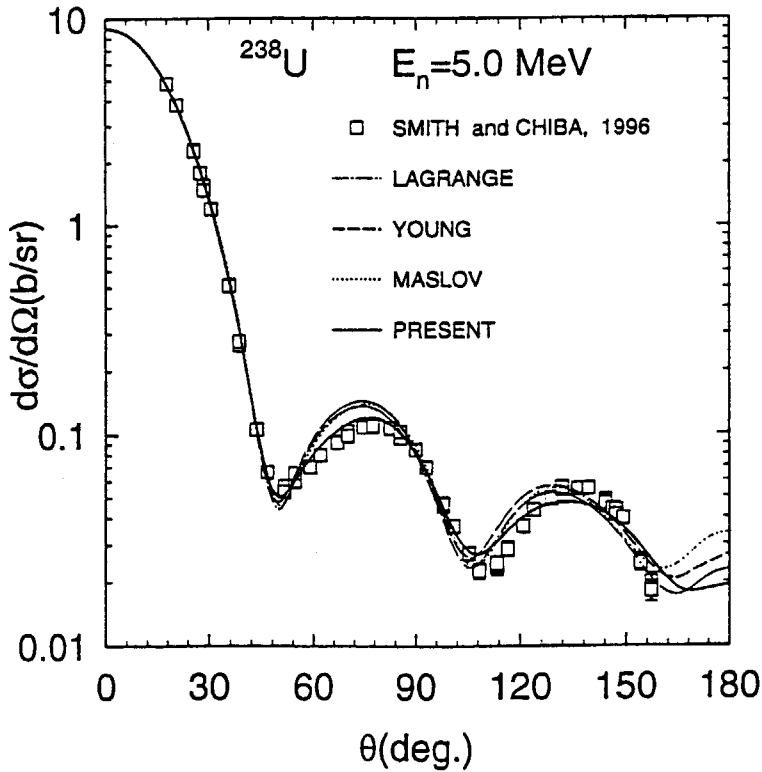


Fig. 6. Same as Fig. 5 but at 5.0 MeV.

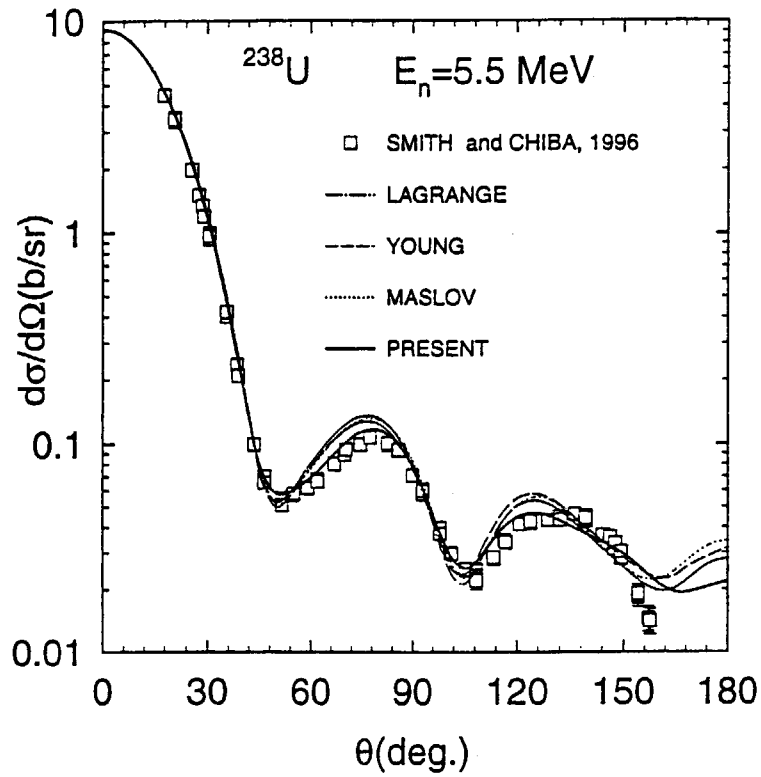


Fig. 7. Same as Fig. 5 but at 5.5 MeV.

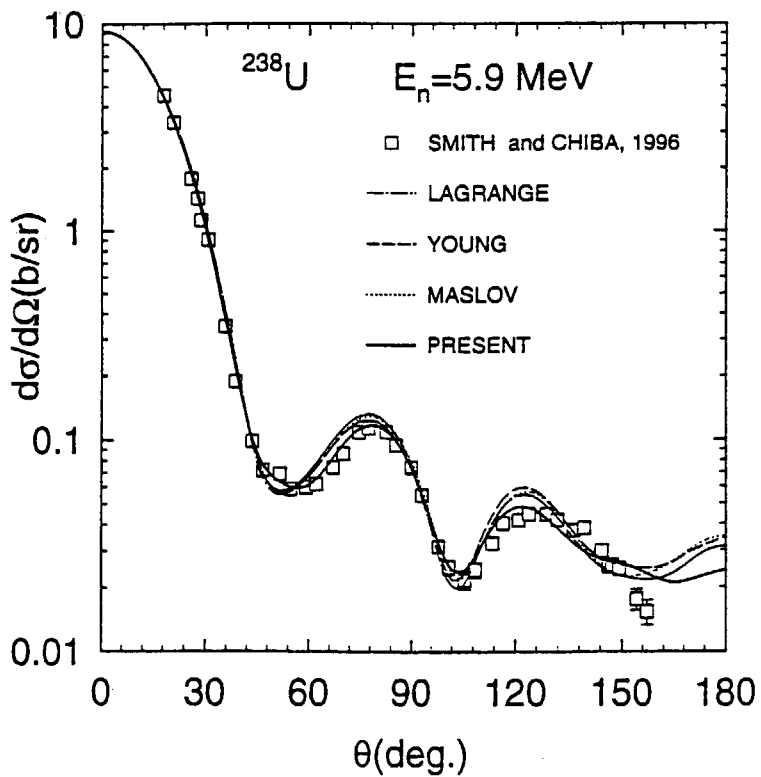


Fig. 8. Same as Fig. 5 but at 5.9 MeV.

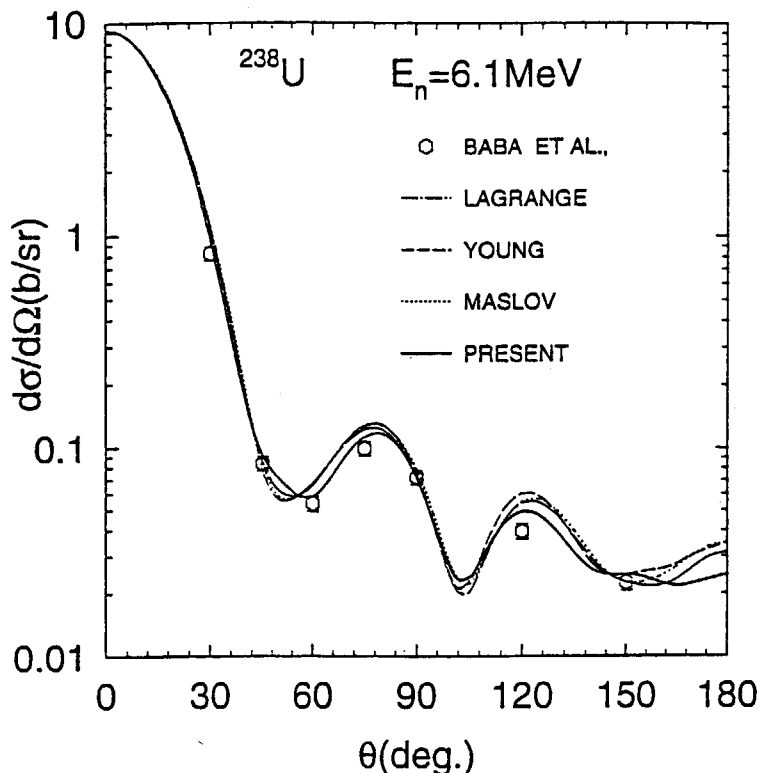


Fig. 9. Neutron scattering cross section for excitation of a sum of 0^+ , 2^+ , 4^+ , 6^+ and 8^+ levels of ^{238}U at 6.1 MeV. The open hexagones denote experimental data obtained by Baba et al. Meanings of the lines are the same as in Fig. 2.

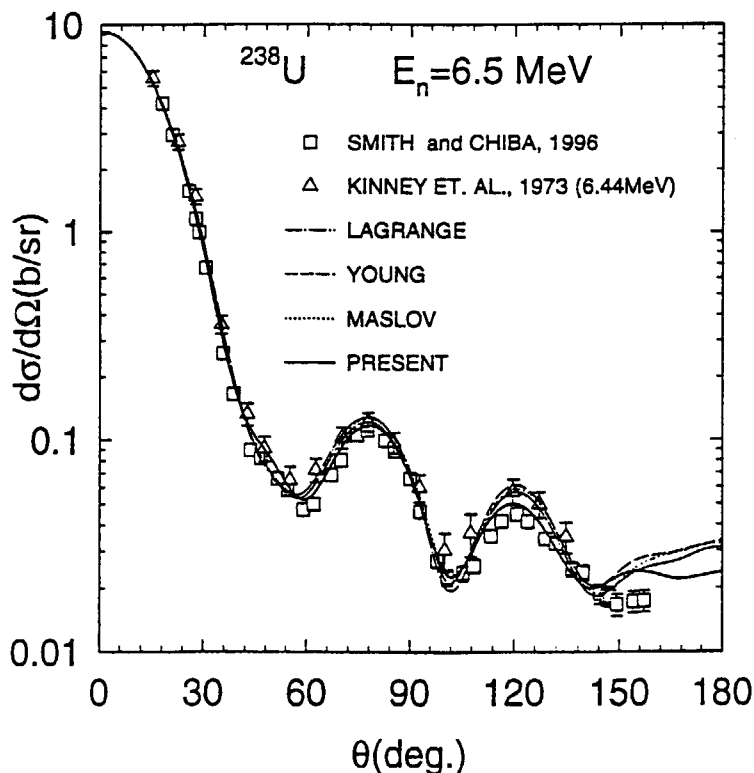


Fig. 10. Neutron scattering cross section for excitation of a sum of 0^+ , 2^+ , 4^+ , 6^+ and 8^+ levels of ^{238}U at 6.5 MeV. The open squares denote experimental data obtained by Smith and Chiba. The open triangles denote experimental data obtained by Kinney et al. Meanings of the lines are the same as in Fig. 2.

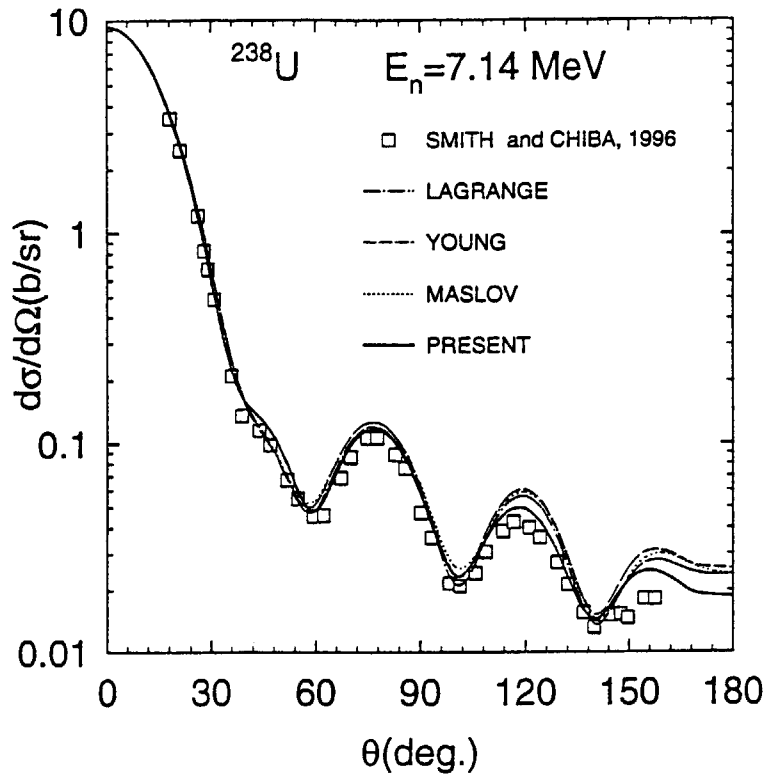


Fig. 11. Same as Fig. 10 but at 7.14 MeV.

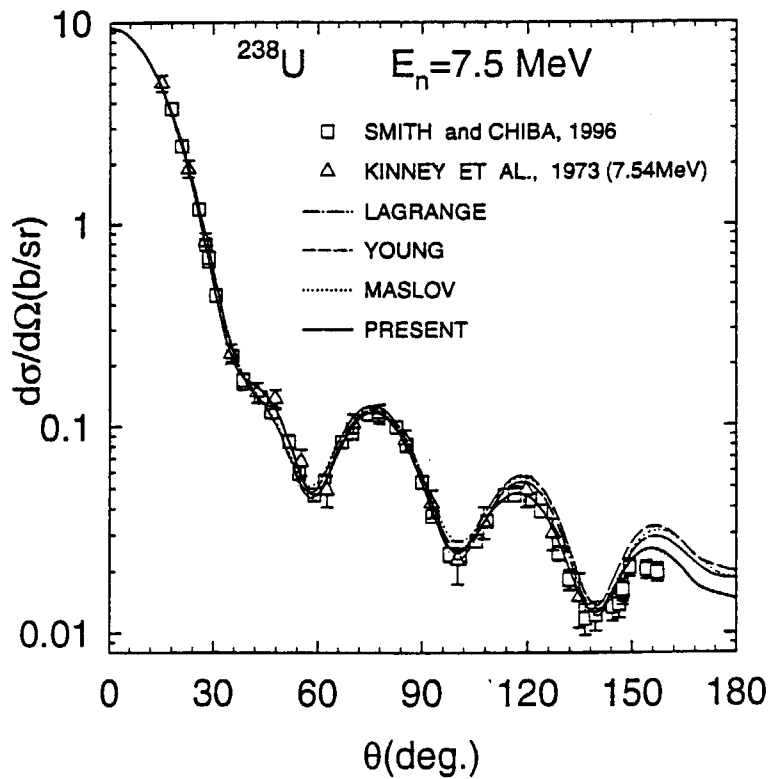


Fig. 12. Same as Fig. 10 but at 7.5 MeV.

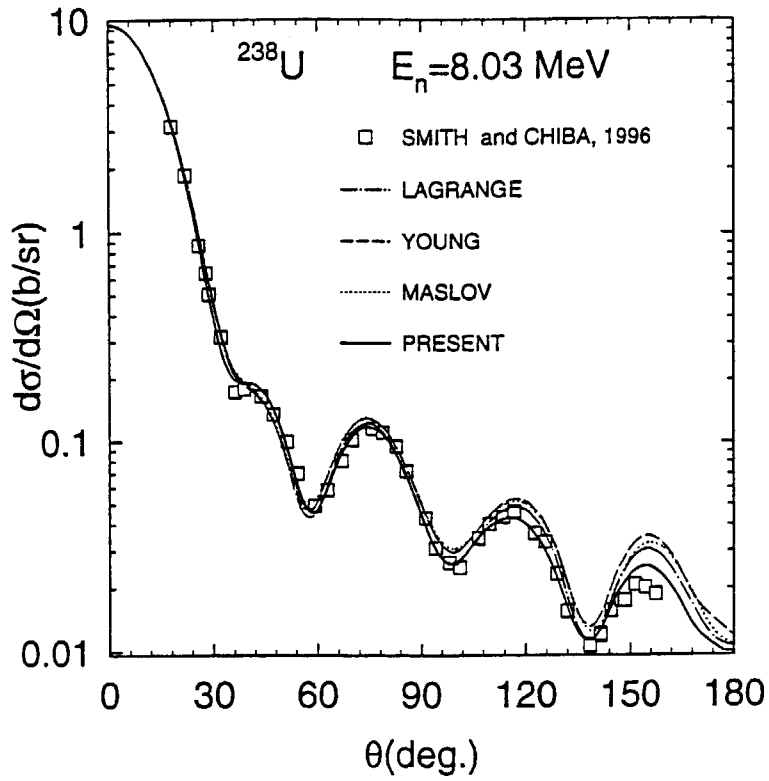


Fig. 13. Same as Fig. 10 but at 8.03 MeV.

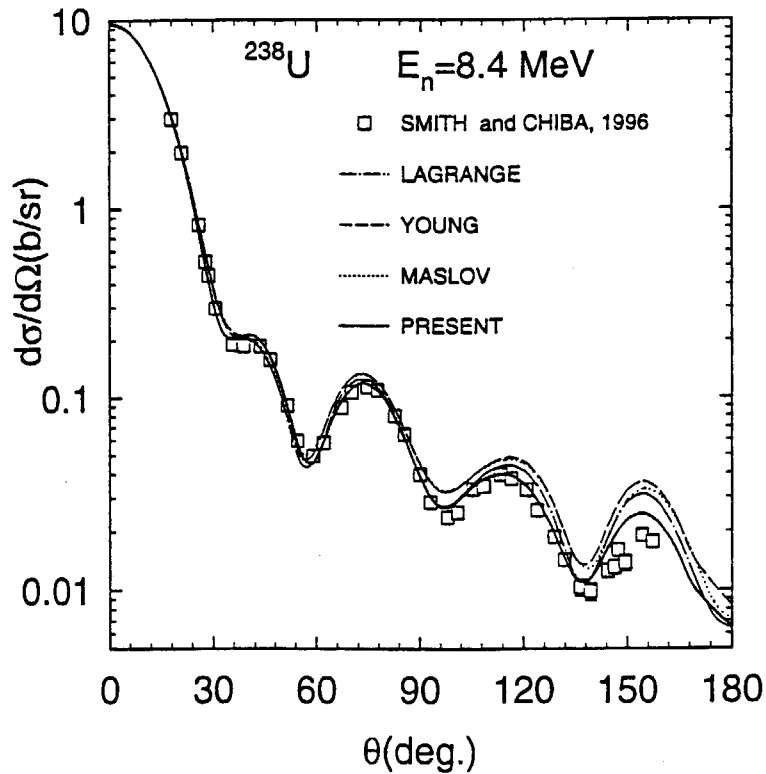


Fig. 14. Same as Fig. 10 but at 8.4 MeV.

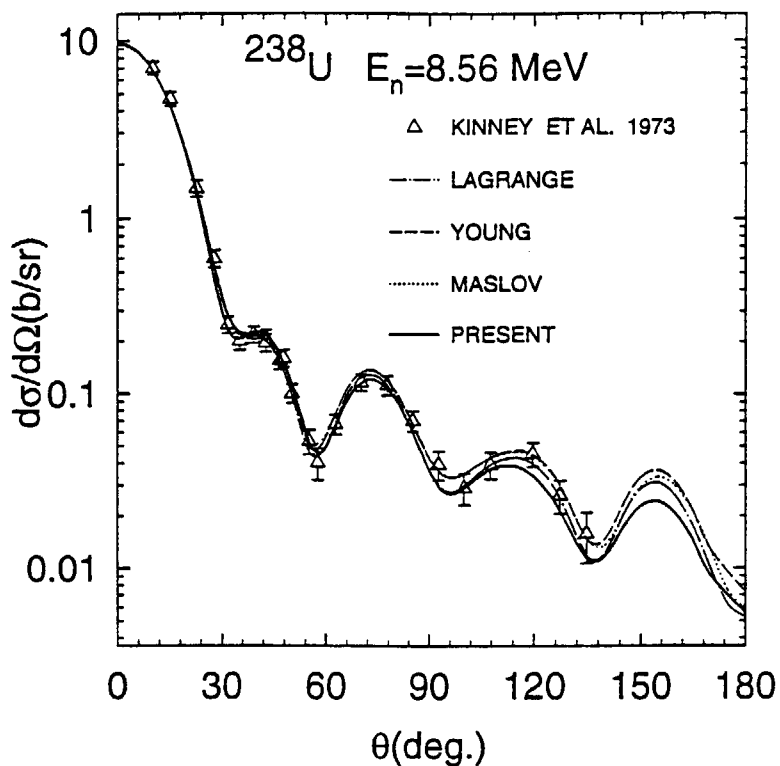


Fig. 15. Neutron scattering cross section for excitation of a sum of 0^+ , 2^+ , 4^+ , 6^+ and 8^+ levels of ^{238}U at 8.56 MeV. The opened triangles denote experimental data obtained by Kinney et al. Meanings of the lines are the same as in Fig. 2.

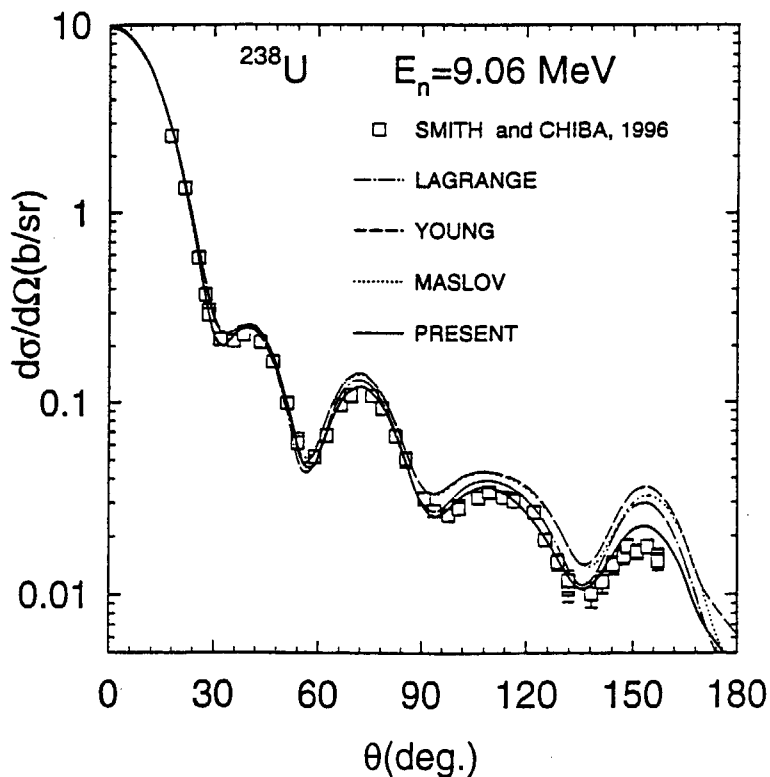


Fig. 16. Same as Fig. 10 but at 9.06 MeV.

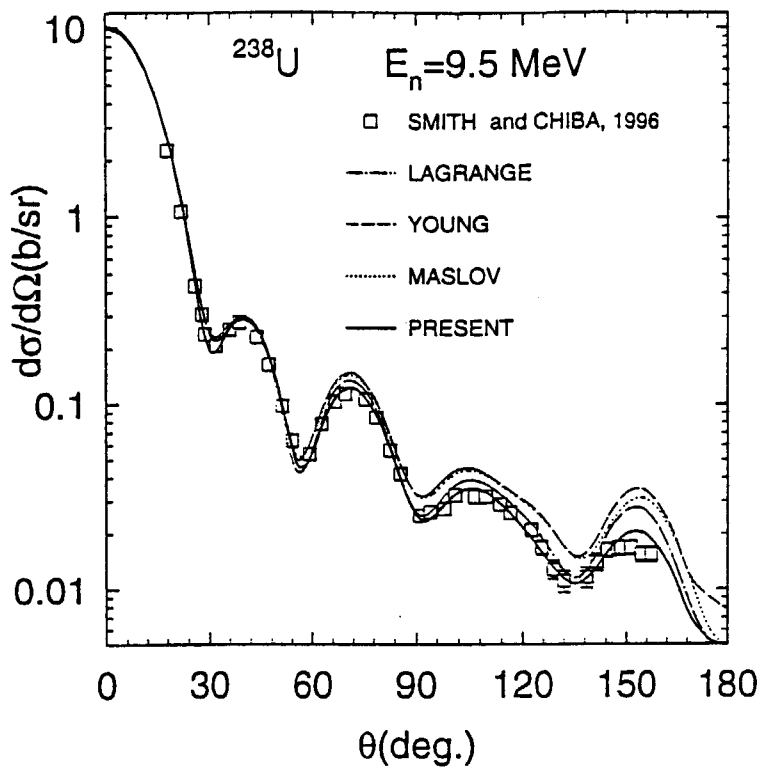


Fig. 17. Same as Fig. 10 but at 9.5 MeV.

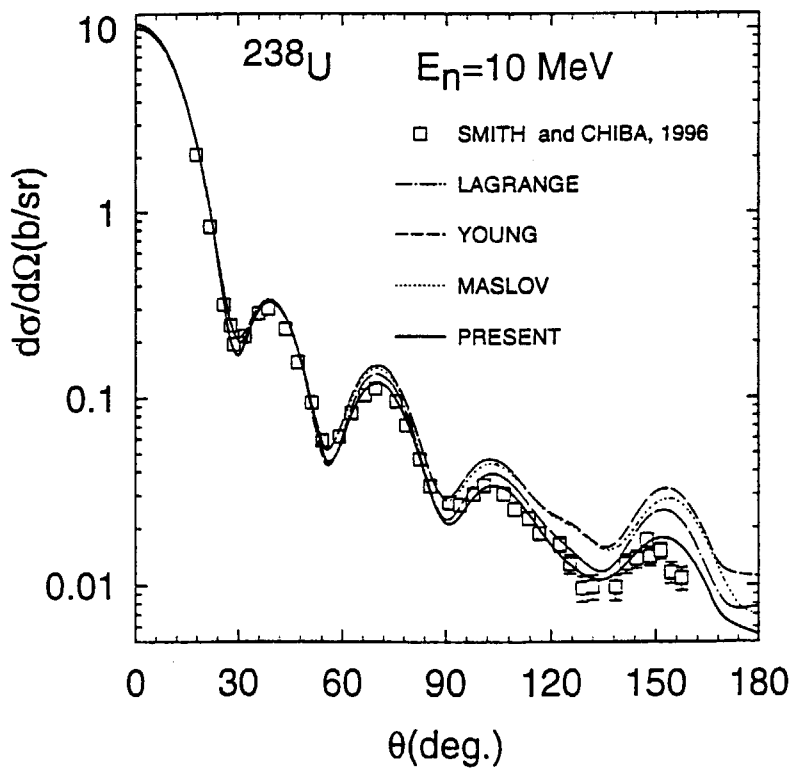


Fig. 18. Same as Fig. 10 but at 10.0 MeV.

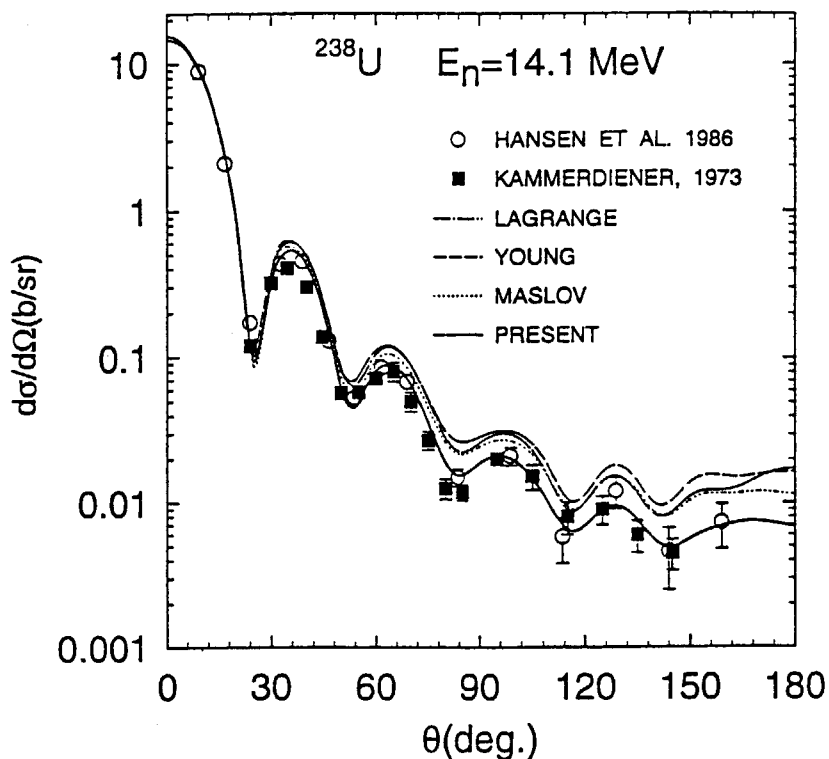


Fig. 19. Neutron scattering cross section for excitation of a sum of 0^+ , 2^+ , 4^+ , 6^+ and 8^+ levels of ^{238}U at 14.1 MeV. The open circles denote experimental data obtained by Hansen et al. while full squares by Kammerdiener. Meanings of the lines are the same as in Fig. 2.

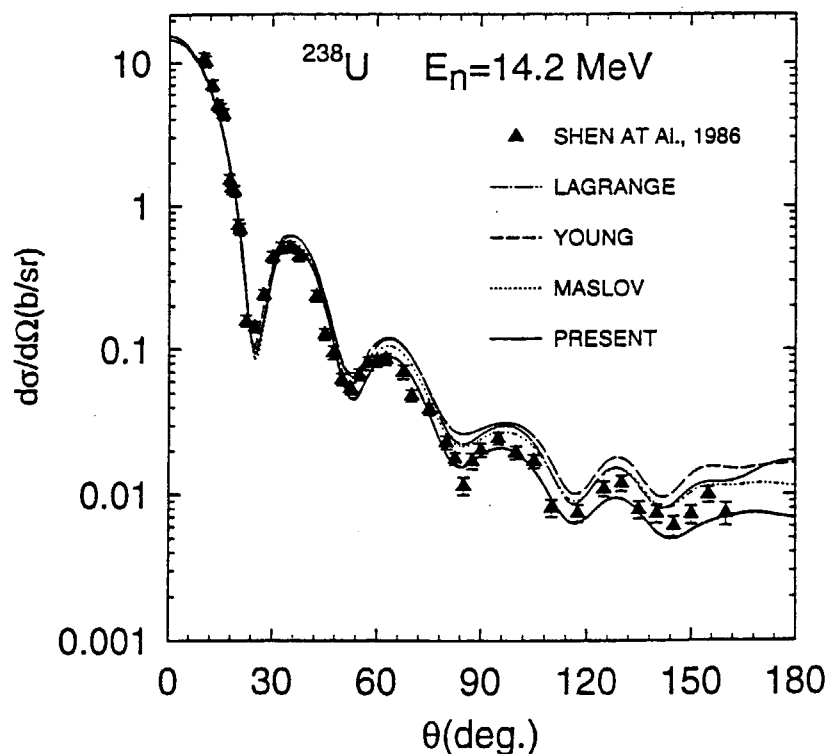


Fig. 20. Neutron scattering cross section for excitation of a sum of 0^+ , 2^+ , 4^+ , 6^+ and 8^+ levels of ^{238}U at 14.2 MeV. The full triangles denote experimental data obtained by Shen et al. Meanings of the lines are the same as in Fig. 2.

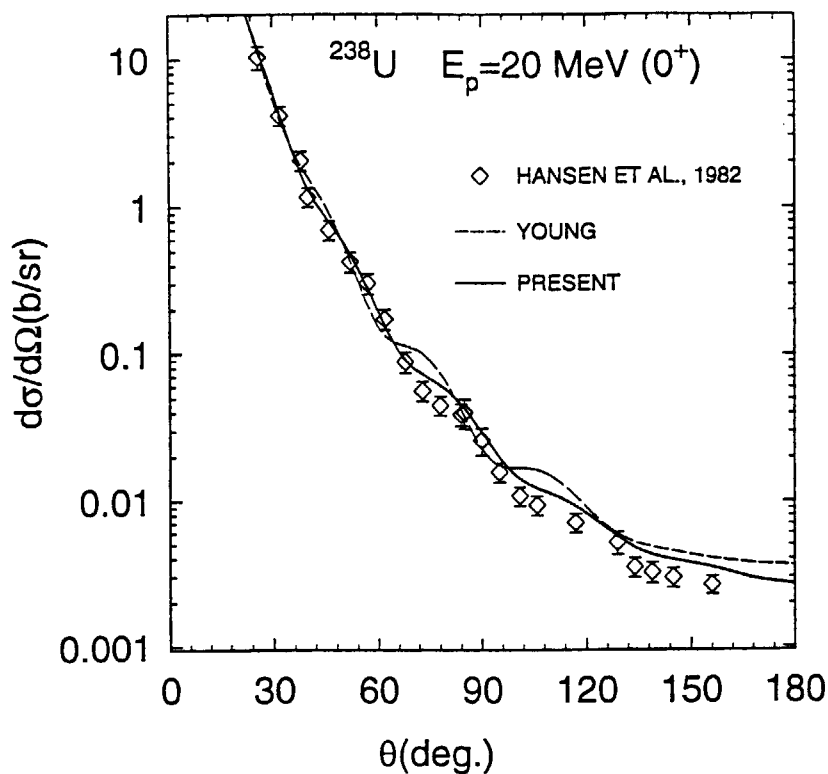


Fig. 21. Proton elastic scattering cross section for ^{238}U at 20 MeV. The open diamonds denote experimental data obtained by Hansen et al. The solid line shows calculated data with the present optical potential, while the broken line with the OMP of Young.

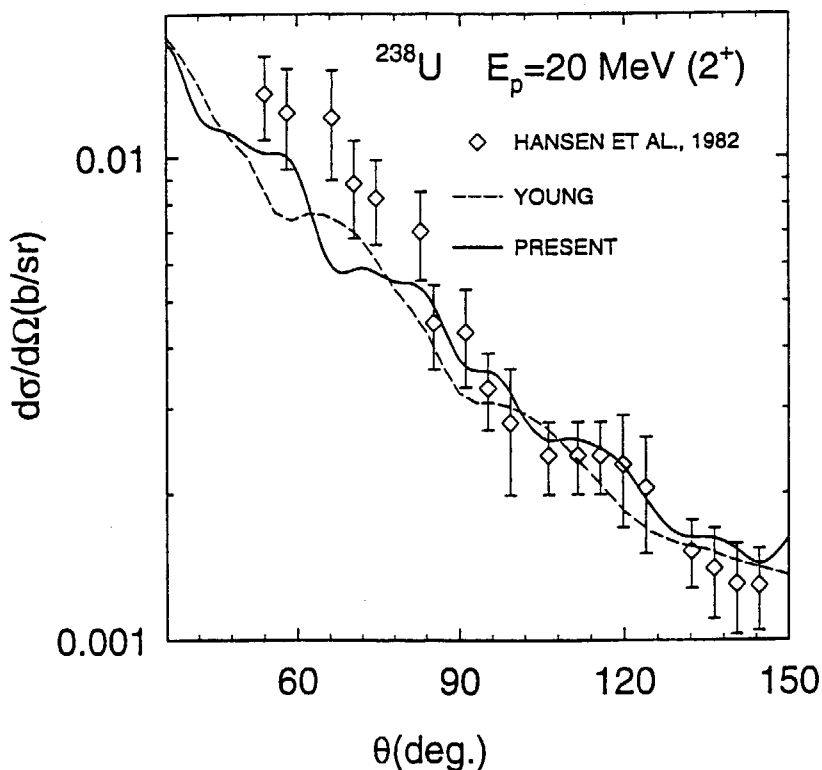


Fig. 22. Proton inelastic scattering cross section to the 1st excited state (2^+) of ^{238}U at 20 MeV. Meanings of the symbols and lines are the same as in Fig. 21.

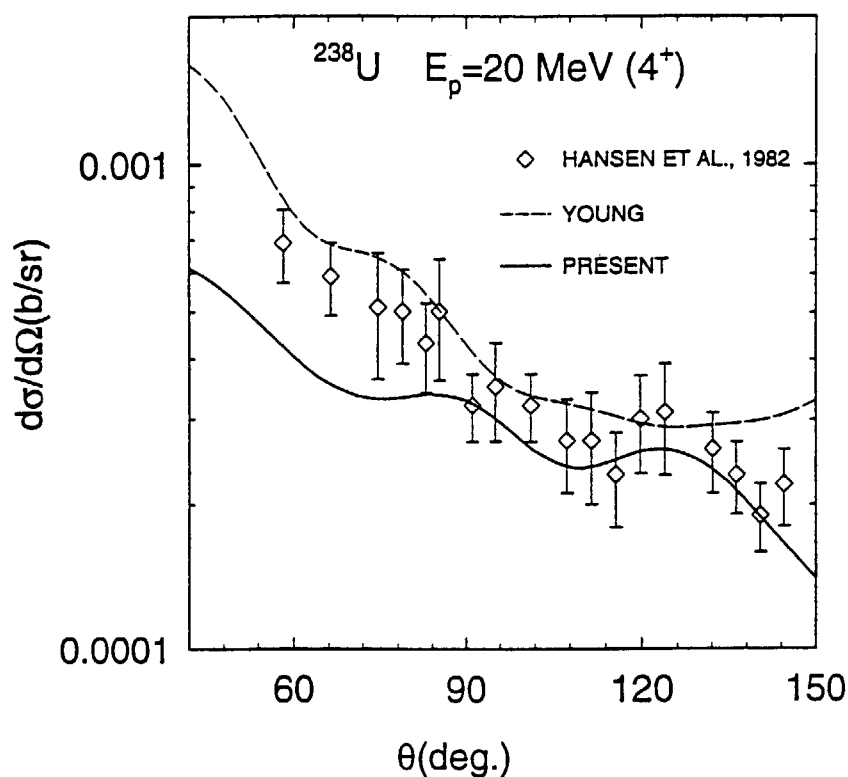


Fig. 23. Proton inelastic scattering cross section to the 2nd excited state (4^+) of ^{238}U at 20 MeV. Meanings of the symbols and lines are the same as in Fig. 21.

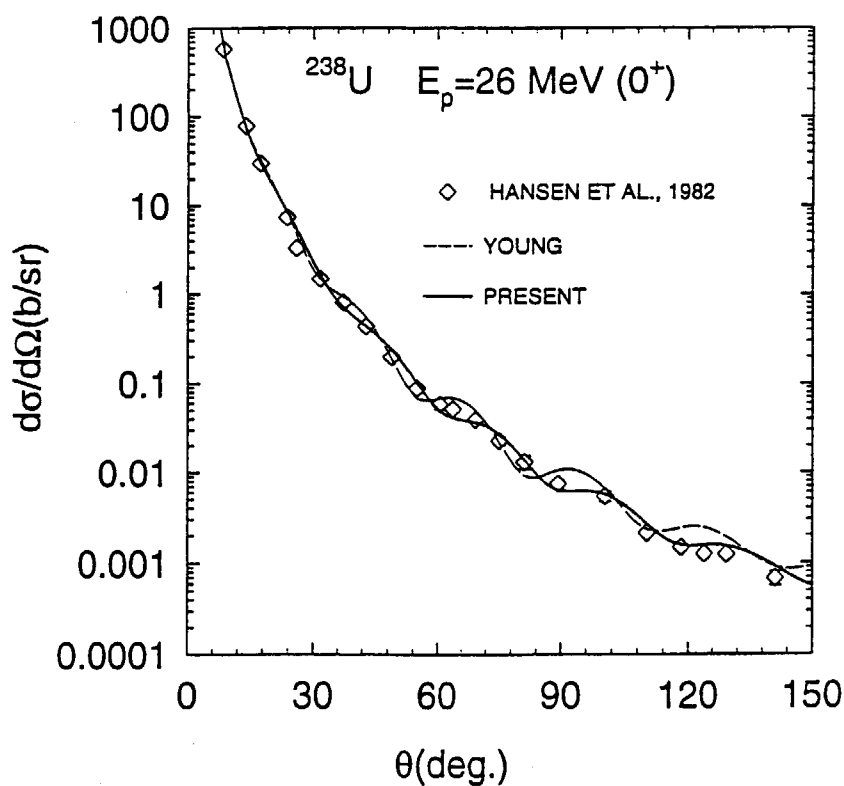


Fig. 24. Proton elastic scattering cross section for ^{238}U at 26 MeV. The open diamonds denote experimental data obtained by Hansen et al. The solid line shows calculated data with the present optical potential, while the broken line with the OMP of Young.

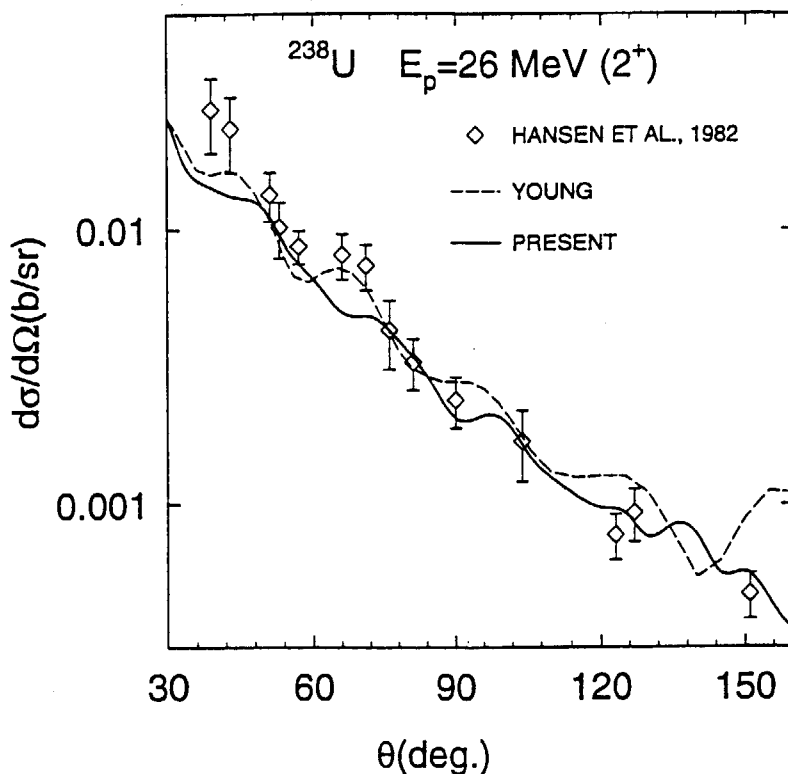


Fig. 25. Proton inelastic scattering cross section to the 1st excited state (2^+) of ^{238}U at 26 MeV. Meanings of the symbols and lines are the same as in Fig. 21.

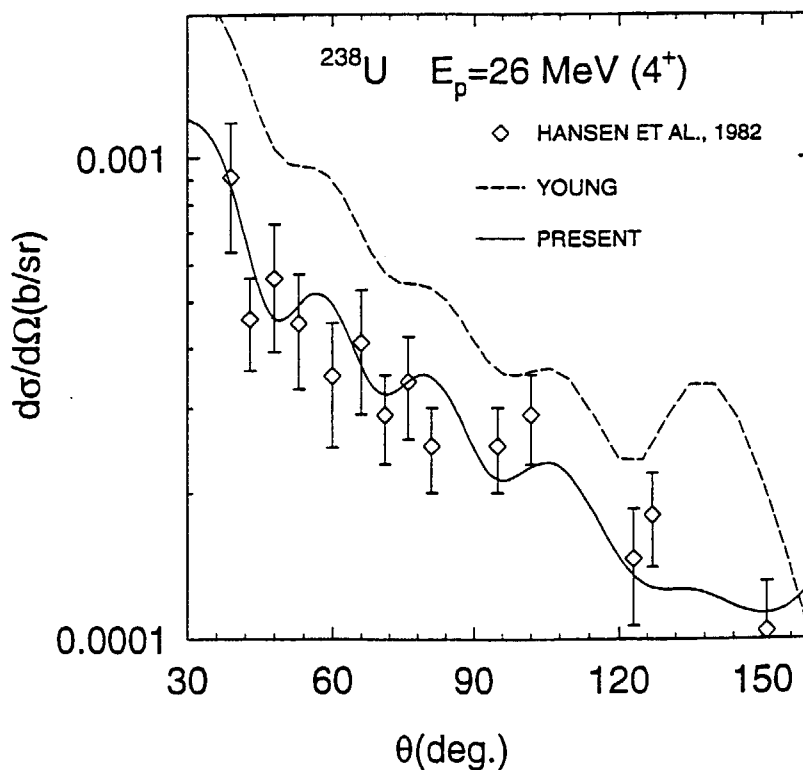


Fig. 26. Proton inelastic scattering cross section to the 2nd excited state (4^+) of ^{238}U at 26 MeV. Meanings of the symbols and lines are the same as in Fig. 21.

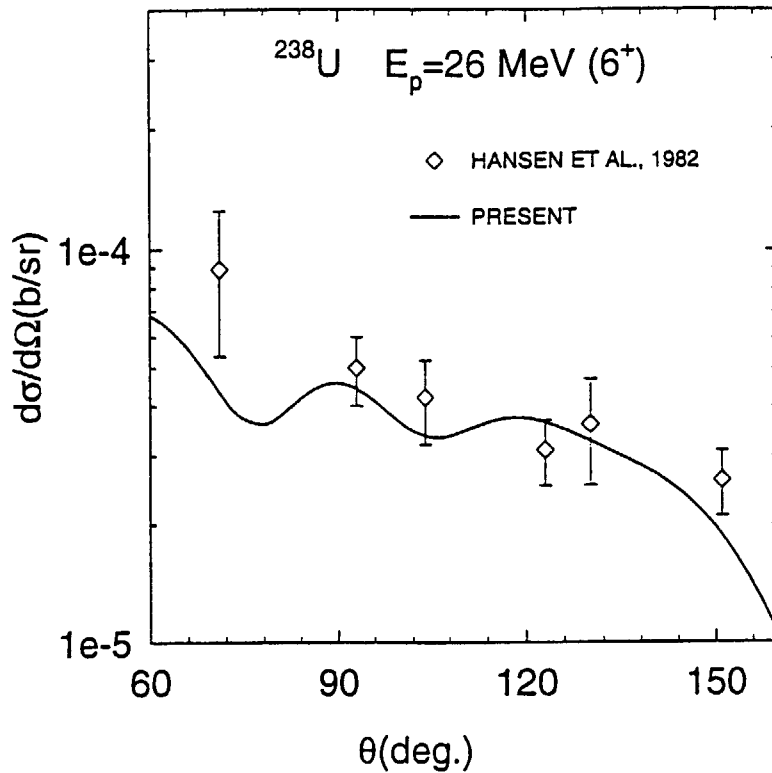


Fig. 27. Proton inelastic scattering cross section to the 3rd excited state (6^+) of ^{238}U at 26 MeV. Meanings of the symbols and lines are the same as in Fig. 21.

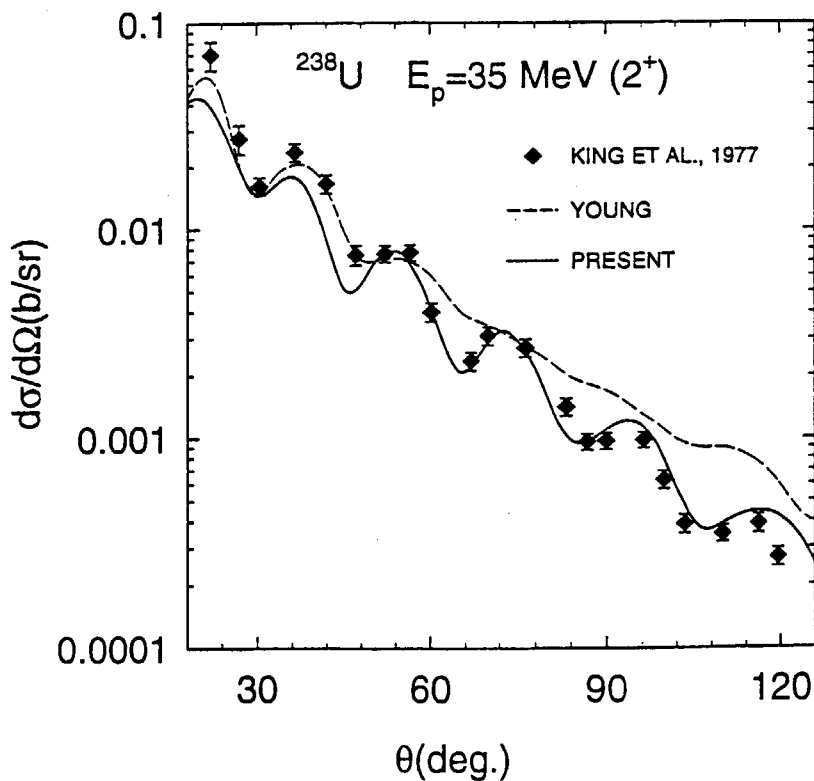


Fig. 28. Proton inelastic scattering cross section to the 1st excited state (2^+) of ^{238}U at 35 MeV. The full diamonds denote experimental data obtained by King et al. The solid line shows calculated data with the present optical potential, while the broken line with the OMP of Young.

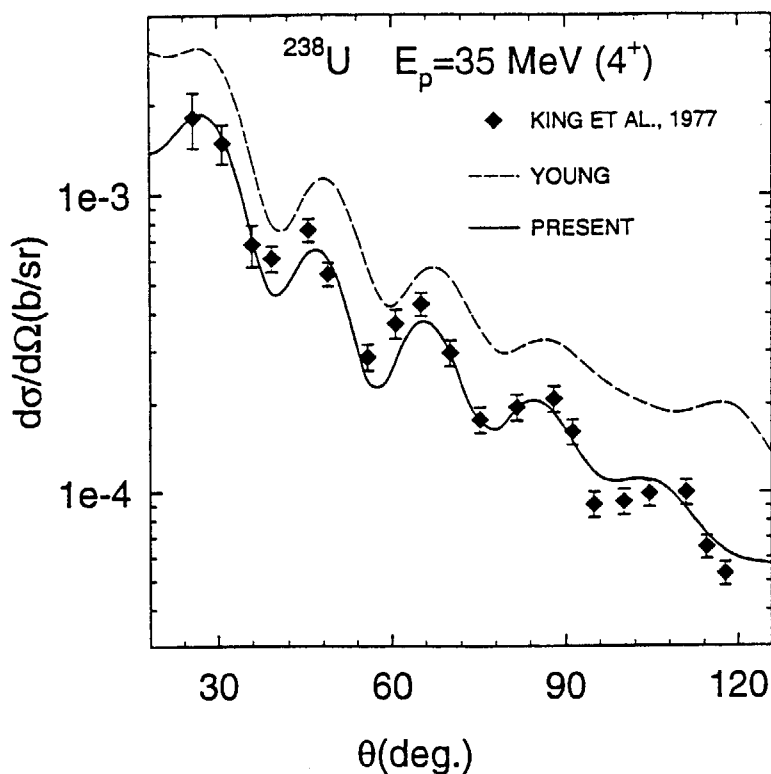


Fig. 29. Proton inelastic scattering cross section to the 2nd excited state (4^+) of ^{238}U at 35 MeV. Meanings of the symbols and lines are the same as in Fig. 28.

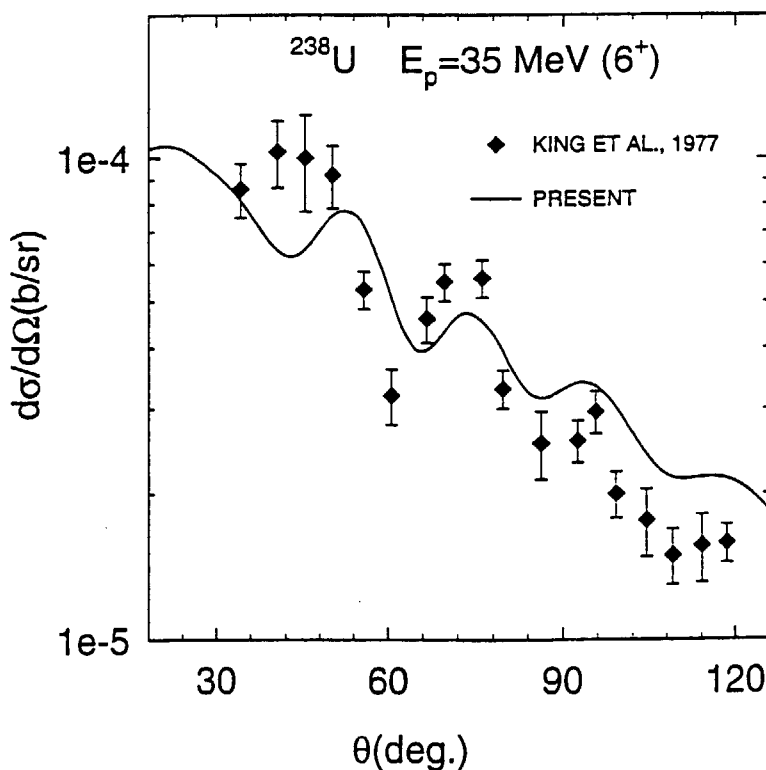


Fig. 30. Proton inelastic scattering cross section to the 3rd excited state (6^+) of ^{238}U at 35 MeV. Meanings of the symbols and lines are the same as in Fig. 28.

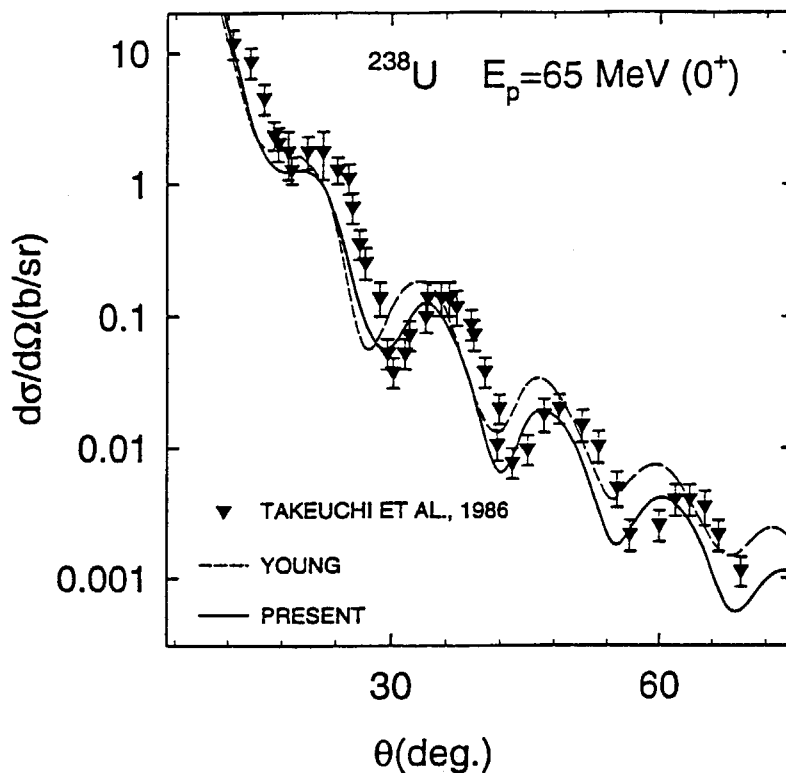


Fig. 31. Proton elastic scattering cross section for ^{238}U at 65 MeV. The reversed full triangles dnote data measured by Takeuchi et al. Meanings of the lines are the same as in Fig. 28.

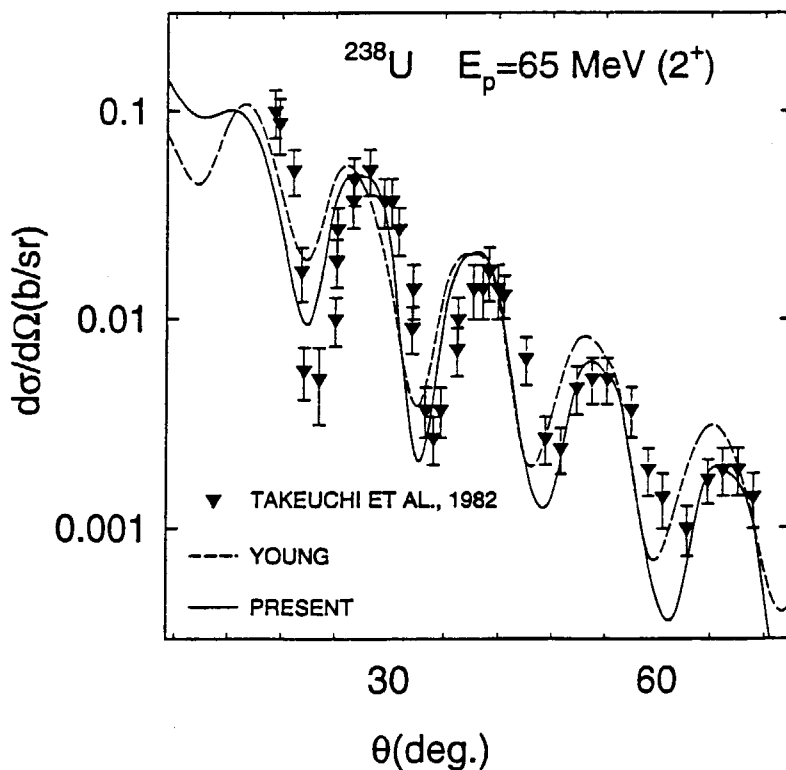


Fig. 32. Proton inelastic scattering cross section to the 1st excited state (2^+) of ^{238}U at 65 MeV. Meanings of the symbols and lines are the same as in Fig. 31.

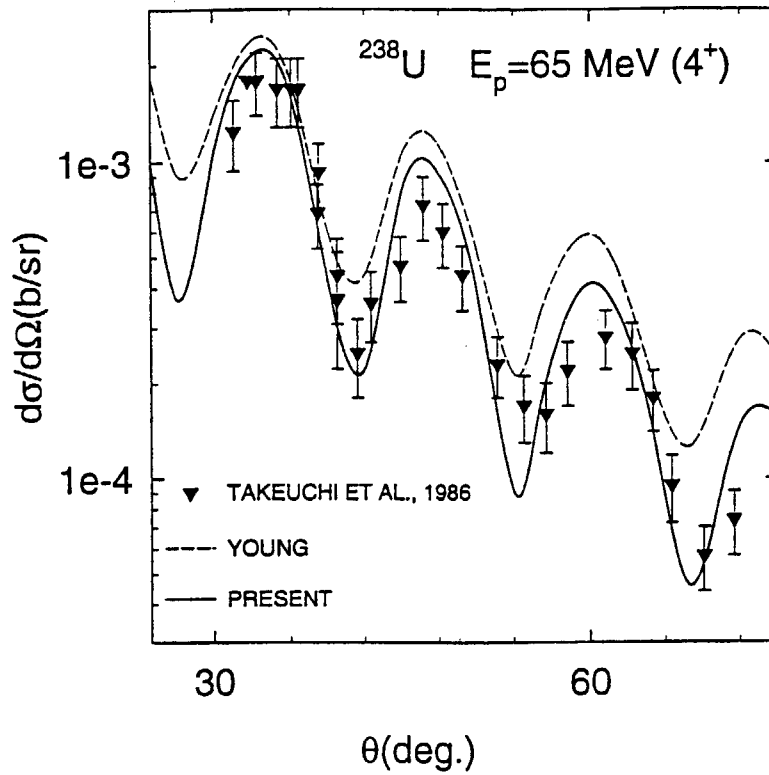


Fig. 33. Proton inelastic scattering cross section to the 2nd excited state (4^+) of ^{238}U at 65 MeV. Meanings of the symbols and lines are the same as in Fig. 31.

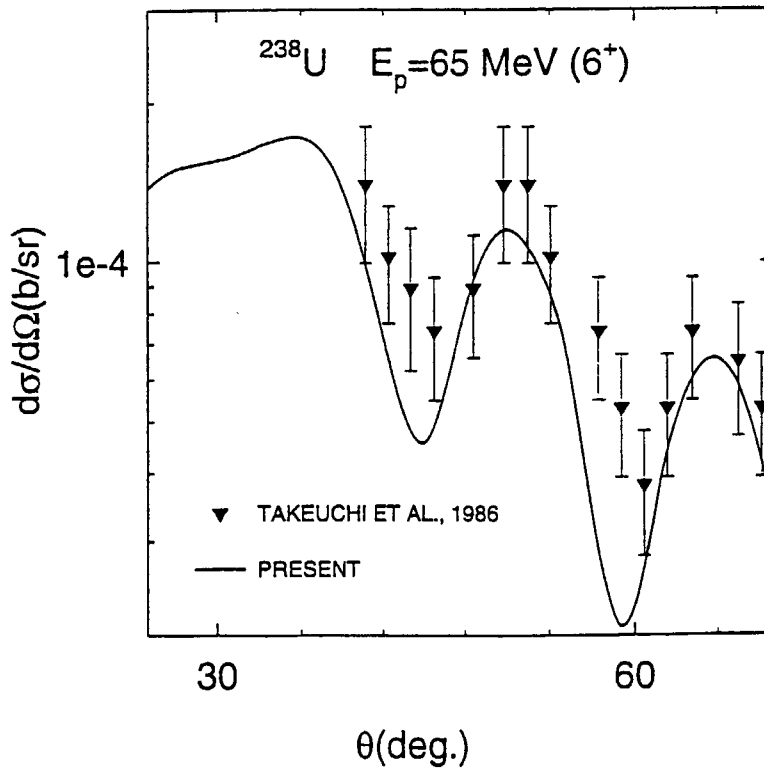


Fig. 34. Proton inelastic scattering cross section to the 3rd excited state (6^+) of ^{238}U at 65 MeV. Meanings of the symbols and lines are the same as in Fig. 31.

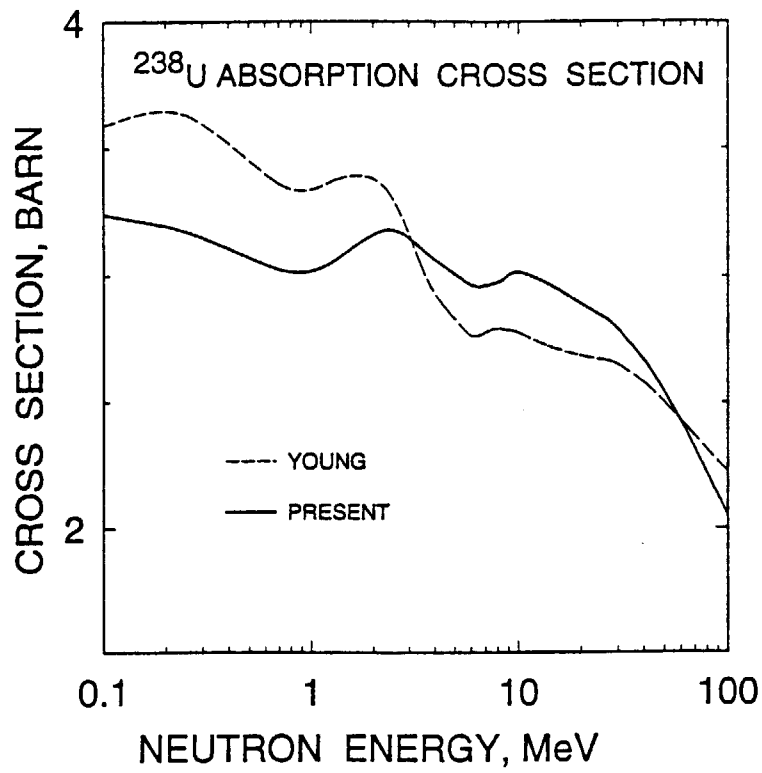


Fig. 35. Neutron absorption cross section of ^{238}U , defined as a difference between the total and sum of direct reaction cross sections. The solid line denotes the calculated result with the present OMP, the broken line with Young's OMP.

国際単位系 (SI) と換算表

表1 SI基本単位および補助単位

| 量 | 名称 | 記号 |
|-------|--------|-----|
| 長さ | メートル | m |
| 質量 | キログラム | kg |
| 時間 | 秒 | s |
| 電流 | アンペア | A |
| 熱力学温度 | ケルビン | K |
| 物質質量 | モル | mol |
| 光度 | カンデラ | cd |
| 平面角 | ラジアン | rad |
| 立体角 | ステラジアン | sr |

表3 固有の名称をもつSI組立単位

| 量 | 名称 | 記号 | 他のSI単位による表現 |
|---------------|--------|----|---------------------|
| 周波数 | ヘルツ | Hz | s ⁻¹ |
| 力 | ニュートン | N | m·kg/s ² |
| 圧力, 応力 | パスカル | Pa | N/m ² |
| エネルギー, 仕事, 熱量 | ジュール | J | N·m |
| 工率, 放射束 | ワット | W | J/s |
| 電気量, 電荷 | クーロン | C | A·s |
| 電位, 電圧, 起電力 | ボルト | V | W/A |
| 静電容量 | ファラド | F | C/V |
| 電気抵抗 | オーム | Ω | V/A |
| コンダクタンス | ジーメン | S | A/V |
| 磁束 | ウェーバ | Wb | V·s |
| 磁束密度 | テスラ | T | Wb/m ² |
| インダクタンス | ヘンリー | H | Wb/A |
| セルシウス温度 | セルシウス度 | °C | |
| 光度 | ルーメン | lm | cd·sr |
| 照射度 | ルクス | lx | lm/m ² |
| 放射線量 | ベクレル | Bq | s ⁻¹ |
| 吸収線量 | グレイ | Gy | J/kg |
| 線量等量 | シーベルト | Sv | J/kg |

表2 SIと併用される単位

| 名称 | 記号 |
|---------|-----------|
| 分, 時, 日 | min, h, d |
| 度, 分, 秒 | °, ', " |
| リットル | l, L |
| トン | t |
| 電子ボルト | eV |
| 原子質量単位 | u |

1 eV=1.60218×10⁻¹⁹J
1 u=1.66054×10⁻²⁷kg

表4 SIと共に暫定的に維持される単位

| 名称 | 記号 |
|----------|-----|
| オングストローム | Å |
| バール | bar |
| ガリ | Gal |
| キュリー | Ci |
| レントゲン | R |
| ラド | rad |
| レム | rem |

1 Å=0.1nm=10⁻¹⁰m
1 b=100fm²=10⁻²⁸m²
1 bar=0.1MPa=10⁵Pa
1 Gal=1cm/s²=10⁻²m/s²
1 Ci=3.7×10¹⁰Bq
1 R=2.58×10⁻⁴C/kg
1 rad=1cGy=10⁻²Gy
1 rem=1cSv=10⁻²Sv

表5 SI接頭語

| 倍数 | 接頭語 | 記号 |
|-------------------|------|----|
| 10 ¹⁸ | エクサ | E |
| 10 ¹⁵ | ペタ | P |
| 10 ¹² | テラ | T |
| 10 ⁹ | ギガ | G |
| 10 ⁶ | メガ | M |
| 10 ³ | キロ | k |
| 10 ² | ヘクト | h |
| 10 ¹ | デカ | da |
| 10 ⁻¹ | デシ | d |
| 10 ⁻² | センチ | c |
| 10 ⁻³ | ミリ | m |
| 10 ⁻⁶ | マイクロ | μ |
| 10 ⁻⁹ | ナノ | n |
| 10 ⁻¹² | ピコ | p |
| 10 ⁻¹⁵ | フェムト | f |
| 10 ⁻¹⁸ | アト | a |

(注)

- 表1-5は「国際単位系」第5版, 国際度量衡局1985年刊行による。ただし, 1eVおよび1uの値はCODATAの1986年推奨値によった。
- 表4には海里, ノット, アール, ヘクトールも含まれているが日常の単位なのでここでは省略した。
- barは, JISでは流体の圧力を表わす場合に限り表2のカテゴリーに分類されている。
- EC閣僚理事会指令では bar, barnおよび「血圧の単位」mmHgを表2のカテゴリーに入れていない。

換算表

| 力 | N (=10 ⁵ dyn) | kgf | lbf |
|---|--------------------------|----------|----------|
| | 1 | 0.101972 | 0.224809 |
| | 9.80665 | 1 | 2.20462 |
| | 4.44822 | 0.453592 | 1 |

粘 度 1Pa·s(N·s/m²)=10P(ポアズ)(g/(cm·s))

動粘度 1m²/s=10⁴St(ストークス)(cm²/s)

| 圧 | MPa (=10bar) | kgf/cm ² | atm | mmHg(Torr) | lbf/in ² (psi) |
|---|--------------------------|--------------------------|--------------------------|-------------------------|---------------------------|
| | 1 | 10.1972 | 9.86923 | 7.50062×10 ³ | 145.038 |
| 力 | 0.0980665 | 1 | 0.967841 | 735.559 | 14.2233 |
| | 0.101325 | 1.03323 | 1 | 760 | 14.6959 |
| | 1.33322×10 ⁻³ | 1.35951×10 ⁻³ | 1.31579×10 ⁻³ | 1 | 1.93368×10 ⁻² |
| | 6.89476×10 ⁻³ | 7.03070×10 ⁻² | 6.80460×10 ⁻² | 51.7149 | 1 |

| エネルギー・仕事・熱量 | J (=10 ⁷ erg) | kgf·m | kW·h | cal(計量法) | Btu | ft·lbf | eV |
|-------------|--------------------------|--------------------------|---------------------------|--------------------------|--------------------------|--------------------------|--------------------------|
| | 1 | 0.101972 | 2.77778×10 ⁻⁷ | 0.238889 | 9.47813×10 ⁻⁴ | 0.737562 | 6.24150×10 ¹⁸ |
| | 9.80665 | 1 | 2.72407×10 ⁻⁶ | 2.34270 | 9.29487×10 ⁻³ | 7.23301 | 6.12082×10 ¹⁹ |
| | 3.6×10 ⁶ | 3.67098×10 ⁵ | 1 | 8.59999×10 ⁵ | 3412.13 | 2.65522×10 ⁶ | 2.24694×10 ²⁵ |
| | 4.18605 | 0.426858 | 1.16279×10 ⁻⁶ | 1 | 3.96759×10 ⁻³ | 3.08747 | 2.61272×10 ¹⁹ |
| | 1055.06 | 107.586 | 2.93072×10 ⁻⁴ | 252.042 | 1 | 778.172 | 6.58515×10 ²¹ |
| | 1.35582 | 0.138255 | 3.76616×10 ⁻⁷ | 0.323890 | 1.28506×10 ⁻³ | 1 | 8.46233×10 ¹⁸ |
| | 1.60218×10 ¹⁹ | 1.63377×10 ²⁰ | 4.45050×10 ⁻²⁶ | 3.82743×10 ²⁰ | 1.51857×10 ²² | 1.18171×10 ¹⁹ | 1 |

1 cal= 4.18605J (計量法)
= 4.184J (熱化学)
= 4.1855J (15°C)
= 4.1868J (国際蒸気表)
仕事率 1 PS(仏馬力)
= 75 kgf·m/s
= 735.499W

| 放射能 | Bq | Ci |
|-----|----------------------|---------------------------|
| | 1 | 2.70270×10 ⁻¹¹ |
| | 3.7×10 ¹⁰ | 1 |

| 吸収線量 | Gy | rad |
|------|------|-----|
| | 1 | 100 |
| | 0.01 | 1 |

| 照射線量 | C/kg | R |
|------|-----------------------|------|
| | 1 | 3876 |
| | 2.58×10 ⁻⁴ | 1 |

| 線量当量 | Sv | rem |
|------|------|-----|
| | 1 | 100 |
| | 0.01 | 1 |

^{238}U OPTICAL POTENTIAL UP TO 100MeV INCIDENT NUCLEON ENERGIES